Tissue stiffening coordinates morphogenesis by triggering collective cell migration *in vivo*

Elias H Barriga[1,3], **Kristian Franze**[2], **Guillaume Charras**[1,3], and **Roberto Mayor**[1,*]

[1]Department of Cell and Developmental Biology, University College London, Gower Street, London WC1E 6BT, UK

[2]Department of Physiology, Development and Neuroscience, University of Cambridge, Downing Street, Cambridge CB2 3DY, UK

[3]London Centre for Nanotechnology, University College London, Gower Street, London WC1E 6BT, UK

Abstract

Collective cell migration (CCM) is essential for morphogenesis, tissue remodelling, and cancer invasion1,2. *In vivo*, groups of cells move in an orchestrated way through tissues. This movement requires forces and involves mechanical as well as molecular interactions between cells and their environment. While the role of molecular signals in CCM is comparatively well understood1,2, how tissue mechanics influence CCM *in vivo* remains unknown. Here we investigated the importance of mechanical cues in the collective migration of the *Xenopus laevis* neural crest cells, an embryonic cell population whose migratory behaviour has been likened to cancer invasion3. We found that, during morphogenesis, the head mesoderm underlying the cephalic neural crest stiffens. This stiffening initiated an epithelial-to-mesenchymal transition (EMT) in neural crest cells and triggered their collective migration. To detect changes in their mechanical environment, neural crest use integrin/vinculin/talin-mediated mechanosensing. By performing mechanical and molecular manipulations, we showed that mesoderm stiffening is necessary and sufficient to trigger neural crest migration. Finally, we demonstrated that convergent extension of the mesoderm, which starts during gastrulation, leads to increased mesoderm stiffness by increasing the cell density underneath the neural crest. These results unveil a novel role for mesodermal convergent extension as a mechanical coordinator of morphogenesis, and thus reveal a new link between two apparently unconnected processes, gastrulation and neural crest migration, via

changes in tissue mechanics. Overall, we provide the first demonstration that changes in substrate stiffness can trigger CCM by promoting EMT *in vivo*. More broadly, our results raise the exciting idea that tissue mechanics combines with molecular effectors to coordinate morphogenesis4.

NC migrates as a mesenchymal cell population, and it has been shown that key transcription factors (e.g. *Snail*, *Twist*, *Zeb*) are sufficient to promote EMT *in vitro*3,5. During development, these factors are expressed well in advance of the onset of NC migration4,6; and it is unclear whether they are sufficient to trigger cell migration or if additional extrinsic factors are also needed. To test if the onset of NC migration is determined by extrinsic factors, we utilized heterochronic tissue grafts to expose non- and pre-migratory NC to embryonic environments at different developmental stages. Here we define non- and pre-migratory NC as those cells that are not migrating (stage 13)7 or are about to start migrating (stage 20)7, respectively (Fig. 1a). When grafted into a host at a migratory stage, non-migratory NC migrated, whereas migration was impaired if pre-migratory NC was grafted into a non-migratory host (Fig. 1b–e; graft controls in Extended Data Fig. 1a–d). Furthermore, when cultured *ex vivo* and exposed to the NC chemoattractant Sdf-1, which controls NC directional migration *in vivo*8, non- and pre-migratory NC were identically motile (Fig. 1f; Supplementary Video 1), indicating that the cells are intrinsically capable of migrating irrespective of their embryonic stage. Together, these observations suggested that changes in environmental factors regulate the onset of NC migration.

One possible source of environmental changes is a modification of the extracellular matrix (ECM). However, between non- and pre- migratory stages, we did not observe changes in Fibronectin, the principal component of *Xenopus* cranial NC ECM9 (Extended Data Fig. 2a–d). As both EMT and cell migration have been shown to be influenced by the mechanical properties of the cellular environment *in vitro*10,11, we next characterized tissue stiffness of developing *Xenopus* embryos using a novel *in vivo* atomic force microscopy (iAFM) approach12. As the cephalic NC use head mesoderm as a substrate for migration, we directly measured its apparent elastic moduli by removing the superficial epidermis (Fig 1g; AFM controls in Extended Data Fig. 2g–j). When comparing stiffness at non- and pre-migratory embryonic stages, stiffness of the mesoderm in front of the NC gradually and significantly increased over time (Fig. 1h). No effect on elastic moduli was observed after removing Fibronectin (Extended Data Fig. 2e,f), confirming that Fibronectin does not contribute to mesodermal stiffness, as previously shown13. Consequently, we found a strong correlation between mesodermal stiffening and the onset of NC migration (R= 0.82, N= 16 animals), suggesting that tissue stiffening may trigger NC CCM *in vivo*.

To test whether these changes in *in vivo* substrate stiffness are sufficient to trigger NC CCM, we cultured NC on Fibronectin-coated hydrogels with stiffness values similar to those found in non- and pre-migratory mesoderm (Extended Data Fig. 2k–m). Remarkably, pre-migratory NC migrated towards Sdf-1 when explanted onto stiff but not onto soft substrates (Fig. 1i;Supplementary Video 2). High resolution imaging revealed that clusters as well as individual NC cells explanted onto stiff substrates formed larger protrusions than those explanted onto soft substrates (Extended Data Fig. 3a–c; Supplementary Video 3). NC clusters, but not single cells, displayed directional motion towards Sdf-1 on stiff substrates

(Extended Data Fig. 3d). These observations suggest that substrate stiffness can be sensed at the single cell level; however, directed motion is an emergent property arising from cell-cell interactions.

Furthermore, NC cultured on stiff, but not on soft, substrates tended to disperse (Extended Data Fig. 3e–h; Supplementary Video 4), a landmark of EMT[14]. Consequently, we found that stiff substrate reduced the levels of the epithelial marker E-cadherin[2,14], whereas the expression of the mesenchymal marker N-cadherin[2,8,14] was increased (Extended Data Fig. 3i,j). Hence, these results suggested that environmental stiffening of the mesoderm may prime NC CCM by triggering EMT.

To confirm that the observed increase in mesodermal stiffness is important for NC migration *in vivo*, we next perturbed mesoderm stiffness using mechanical and molecular manipulations. Most developmental systems are under tension[15,16], which can lead to strain stiffening of the tissue, increasing its apparent elastic modulus[12,17–19]. To decrease the stiffness experienced by NC cells, we mechanically ablated its surrounding tissue, leading to a release of tension and hence to a decrease in strain stiffening. Tissue ablation in the anterior region of the embryo (Fig. 2a) led to reduced mesodermal stiffness compared to non-ablated side, as recorded by iAFM (Fig. 2b) and it inhibited NC migration (Fig. 2c, d; ablation controls in Extended Data Fig. 4a, b).

Next, we molecularly manipulated mesoderm stiffness by performing targeted injections of myosin activity inhibitors, which decrease tissue stiffness (Fig. 2e,f and Extended Data Fig. 4c–d). The injection of either a translation blocking morpholino against Myosin-light-chain 9 (Myl9) or a constitutively active form of myosin phosphatase (CA-MYPT) significantly decreased mesoderm stiffness and blocked NC migration, as shown by *in situ* hybridisation of the migratory NC marker *snail2* (Fig. 2f–i). A similar inhibition of NC migration was observed in embryos in which wild-type NC were grafted into embryos injected with Myl9MO or CA-MYPT (Extended Data Fig. 5a–d; Fibronectin deposition control in Extended Data Figure 6a–g), ruling out an effect of the manipulation of myosin on the NC cells' migratory capacities. These data show that reaching a critical stiffness in the mesoderm is required to promote NC migration *in vivo*.

We next investigated whether reaching such threshold stiffness in non-migratory embryos was sufficient to trigger premature NC migration. Injection of a constitutively active form of myosin light chain (CA-MLC) into the mesoderm led to an early increase in tissue stiffness equivalent to that reached in pre-migratory embryos, and it promoted premature NC migration (Fig. 2j–l; Extended Data Fig. 5e–g). To increase tissue stiffness without genetic or pharmacological manipulations we locally applied a sustained compressive force on the embryos using iAFM (Fig. 2m; compression controls in Extended Data Fig. 4e–i), leading to strain stiffening[12,18,19]. These results demonstrated that mesodermal stiffening is necessary and sufficient to trigger collective migration of the NC *in vivo*.

To test how NC cells sense this increase in mesodermal stiffness, we perturbed signalling by inhibiting the Integrin/Vinculin/Talin complex, which mediates mechanosensing in other systems[20]. We inhibited the integrin pathway in the NC by using a morpholino against Itgβ1

(Itgβ1-MO) and negative dominants for Vinculin and Talin. Inhibition of any of these mechanosensors led to a strong impairment of the onset of NC migration *in vivo* (Extended Data Fig 7a–c), without significantly affecting attachment *in vitro*. These results show that the NC requires integrin/vinculin/talin for its migration, suggesting that this pathway is involved in NC mechanosensing.

Our next goal was to examine the mechanisms underlying mesodermal stiffening *in vivo*. Modifications in ECM have been proposed to affect tissue stiffness (e.g. increase in collagen fibers)[21,22]; however, collagen is not expressed in the tissue during NC migration[23]. Together with our data (Extended Data Fig. 2a–f) this suggest that changes in ECM are unlikely the cause of mesoderm stiffening in this system.

Although it has been proposed that myosin contractility locally increases tension and thus stiffness of the dorsal mesoderm[13], our control experiments (Extended Data Fig 8a–e; 9a–h) suggest that actomyosin contractility is not essential for controlling head mesodermal stiffness during the stages at which the NC migrates. However, when we inhibited myosin in non-migratory embryos, it reduced mesoderm stiffening and impaired NC migration (Fig 2f–I, Extended Data Fig. 9a, b, c). This temporal difference in action is likely due to the requirement of myosin activity for the migration of mesoderm cells taking place between non- and pre-migratory stages[13,24], which in turn indirectly affect mesoderm stiffness later.

Another factor that controls tissue stiffness is cell density[12,25,26]. During development mesoderm cells accumulate and intercalate in dorsal regions via convergent extension (CE)[24]. To test whether mesodermal cells are accumulated underneath the NC, we measured mesodermal cell densities from non-migratory to pre-migratory stages. Cell densities indeed increased towards the onset of NC migration (Fig. 3a-c), furthermore, cell density directly correlated with mesoderm stiffening in all the treatments that affected migration (R= 0.86, N= 16 animals) (Fig. 3d). These observations confirm that once cells are accumulated by CE, the main contribution to mesoderm stiffness is cell density.

To validate the role of CE in mesoderm stiffening, we specifically inhibited the planar cell polarity pathway (PCP) in the mesoderm with targeted injections of the PCP inhibitor DshDEP[+][24]. Inhibition of PCP signalling impaired NC migration in a non-autonomous manner, as shown by *in situ* hybridization and graft experiments (Fig. 3e–g; Extended Data Fig. 5h–k; Fibronectin controls in Extended Data Fig 6c,f). In agreement with our hypothesis, cell densities and mesoderm stiffness where reduced in DshDEP[+] injected embryos (Fig. 3h–k).

To confirm that the inhibition of NC migration after blocking PCP is a consequence of a mechanical change in the tissue, we rescued mesodermal stiffness in the softer PCP-depleted embryos by applying a sustained extrinsic compression with iAFM (Fig. 4a)[12,18,19]. This was sufficient to completely rescue NC migration (Fig. 4b–d), and to promote premature NC migration (Extended Data Fig. 10). These results indicate that the impaired NC migration observed in PCP-depleted embryos was mainly due to the decreased mesodermal stiffness.

While previous *in vitro* studies proposed that mechanical cues may promote EMT[10] and CCM[11], we here show that CE of the mesoderm leads local stiffening, which in turn works

as a long-range signal triggering EMT and CCM of the NC *in vivo* (Fig. 4e). It is well-known that tissue mechanics are a key determinant in many biological processes, such as axon growth12, central nervous system development25, and maintenance of tissue integrity via cell-cell adhesion during collective cell movement15,16,27,28. The most common regulators of tissue stiffness include ECM accumulation21,22, cortical contractility13,16,17, and cell densities12,25,26. We here identified cellular rearrangements driven by PCP-dependent CE as mechanism that increases cell densities to elevate stiffness in a developing organism. Similar changes in tissue stiffness are likely to occur in other systems undergoing PCP-dependent CE.

An exciting new area of research is related to the *in vitro* generation of organ-analogous structures called organoids4,29,30. This research has focused mainly on the molecular manipulation of homogenous cell populations and mechanical inputs are just starting to be considered in the field29,30. As our findings reveal that proper morphogenesis requires mechanical interaction between different tissues, we anticipate that the consideration of mechanical signals in the organoid field will increase the success of *ex vivo* engineered tissues. Moreover, as CCM is a common mode of migration during development, regeneration, wound healing, and cancer progression1,2,15,16,24,28, it is tempting to speculate that mechanical cues from the surrounding tissues could also play an important role during CCM in these systems.

Methods

Xenopus manipulation, in situ hybridization, and *in vitro* transcription

Xenopus embryos were obtained as previously described14. Briefly, ovulation on mature females was induced by injecting serum gonadotrophin (Intervet) and chorionic gonadotrophin (Intervet). Released eggs were collected and fertilized *in vitro* by mixing with a sperm solution. Embryonic stages were determined by following Nieuwkoop and Faber (1967)7. For in situ hybridizations, an antisense digoxigenin-labeled RNA probes against *snail2*31, a neural crest marker was used and embryos at non-migratory, pre-migratory or migratory stages were fixed, hybridized and stained as with stablished protocols32. Templates for Riboprobes and mRNAs were generated as previously described14,32. In brief, for mRNA transcription a mMESSAGE mMACHINE® SP6 Transcription Kit (Thermo-Fisher AM1340) was used. The riboprobe against *snail2* was transcribed with a Riboprobe® *in vitro* Transcription System (Promega P1420). All animal experiments were approved by the Biological Service Unit at University College London and complied with UK Home Office guidelines (Animal Act 1986).

Morpholino and mRNA injections, and reagents

Microinjections were performed using calibrated needles as described in33. Fertilized eggs were de-jellied for 5 min with a solution containing 1 gr of cysteine (Sigma) and 1 ml of 5N NaOH in 50 ml of ddH$_2$O. For cell labelling 10 nl of nuclear-RFP (nRFP) and/or membraneGFP (mGFP) mRNAs were injected at 2-cell stages in 1 blastomere (250 pg per embryo each construct). Vinculin-Cter and Talin-Nter were previously validated34 and injected at 8 cell-stage in 1 dorsal blastomere (500 pg per embryos each construct). Itgb1-

MO (5'-GAATACTGGATAA- CGGGCCATCTTA-3') was injected as previously published[35] and synthesised by GeneTools (GeneTools, OR, USA). For targeted injections to the mesoderm, 2 dorso-vegetal blastomeres were injected (as shown in Fig. 2 e and Extended Data Fig. 4c). Embryos were injected with 5 pg per blastomere of a morpholino against Myl924 (Myl9-MO 5'-TGGCTTTTGTCTTCTTGCTGGACAT-3'), synthesised by GeneTools (GeneTools, OR, USA); 1 ng per blastomere of DshDEP[+24]; 1 ng per blastomere of a constitutively active form of the myosin regulatory chain phosphatase (CA-MYPT)36; or 1 ng per blastomere of a constitutively active for of myosin regulatory chain (CA-MLC)37, both kindly provided by Dr. Masa Tada.

Blebbistatin incubations: embryos were incubated as indicated on Extended Data Fig. 9, in a solution containing 100 μM blebbistatin (ab12042) dissolved in dimethyl sulfoxide (DMSO, Thermo-Fisher).

Ex vivo neural crest (NC) culture, chemotaxis assay on glass, and graft experiments

Neural crests were dissected at non-migratory or pre-migratory stages as previously described[14]. Briefly, 20 min prior dissection the chorion was removed with fine forceps, embryos were placed in a dish containing modelling clay, and a hair knife was used to remove the epidermis and explant the NC. After dissection, neural crests were maintained in Danilchik's medium (DFA, 53 mM NaCl, 5 mM Na_2CO_3, 4.5 mM KGluconate, 32 mM NaGluconate, 1 mM $MgSO_4$ ($7H_2O$), 1 mM $CaCl_2$, 0.1% BSA; adjusted to pH 8.3 with 1M Bicine). To test the response of NC to Sdf-1 we used a novel chemotaxis assay 8,38, in which acrylic Heparin beads (Sigma-Aldrich) were coated overnight with 1μg/ml Sdf-1 (Sigma-Aldrich), washed with PBS and fixed to a fibronectin-coated glass-bottom dish (μ-Dish 35mm high, Ibidi) using silicon grease. Fluorescently labelled explants (mRFP/mGFP) were placed 2 diameters away from the bead and migration was recorded by time-lapse.

For grafts experiments, wild type or treated NC from donor and hosts embryos were removed as described above, a hair knife was used to locate the donor NC in the host embryo and a piece of glass-coverslip was used to hold the grafted NC. The coverslip was removed after 1 hour and the embryos were mounted for live imaging. Embryos were mounted on agarose dishes containing 1.2 mm lanes with 4% Methyl Cellulose (Sigma-Aldrich) and filled with DFA medium.

Polyacrylamide (PAA) hydrogels preparation and functionalization

Polyacrylamide gels were prepared as follow. To allow adhesion to PAA, glass slides of 76 mm x 24 mm were coated overnight (ON) and at room temperature (RT) in a solution containing 14:1:1 Ethanol: Acetic Acid: PlusONE Bind-Silene® (GE Healthcare) v/v/v. The slides were washed twice with 70% ethanol, air dried and stored at RT. For hydrophobic coating, 13-mm diameter x 0.1 mm glass coverslips were air cleaned and coated for 15 minutes at RT with PlusONE Repel-Silene® ES (GE Healthcare), coverslips were carefully recovered, air-dried and immediately used.

Polyacrylamide mixes were prepared as follow. For soft gels a mix containing 550 μl 7.6 mM HCl, 369.5 μl ddH$_2$O, 0.5 μl of N,N,N′,N′-tetramethylethylenediamine (TEMED, Sigma), 16 μl bis-acrylamide (BioRad), and 60 μl of acrylamide (BioRad) was prepared. For

stiff gels a mix containing 550 μl 7.6 mM HCl, 349.5 μl ddH$_2$O, 0.5 μl of N,N,N′,N′-tetramethylethylenediamine (TEMED, Sigma), 20 μl bis-acrylamide, and 75 μl of acrylamide was prepared. Polymerisation was started by adding 5 μl of 10% Ammonium persulfate (APS, GE Healthcare) to each mix.

Soft or stiff gels were obtained by placing a 12 μl drop of PAA mix on an adhesive slide and covering with a hydrophobic coverslip. Polymerization was allowed for 25 min at RT in a humidifier and the coverslip was carefully removed. Gels were washed 3 times for 10 min with 10 mM HEPES buffer.

fibronectin was covalently linked to soft or stiff gels via Sulfo-SANPAH mediated succinimide cross-linking. To activate gels, aliquots containing 1 mg of Sulfo-SANPAH (Thermo-Fisher 22589) on 20 μl of anhydrous dimethyl sulfoxide (DMSO, Thermo-Fisher D12345), were rapidly diluted on 480 μl of 10 mM HEPES buffer. 25 μl of this dilution was added to the gel surface and gels were irradiated with UV light for 5 min. The excess of Sulfo-SANPAH was removed by washing 5 min with 10 mM HEPES buffer. A drop containing 10 mg/ml of fibronectin was added to the surface of the activated gels, covered with Parafilm, and incubated for 2 hours in a humidifier. Parafilm was removed and the functionalized gels washed twice for 5 min on 10 mM HEPES buffer. Young modulus' [Pa] for each gel were determined by atomic force microscopy and functionalization was checked by immunostaining against fibronectin (Extended Data Figure 2k–m).

Chemotaxis and dispersion assays on hydrogels with varying stiffness values

Chemotaxis—To test how substrate stiffness, contribute to the response of NC cells towards Sdf-1 we developed a novel chemotaxis assay on PAA gels of varying stiffness. In brief, once coated with Sdf-1 as described for the glass chemotaxis assay, acrylic Heparin beads (Sigma-Aldrich) were split in two halves and each halve was gently indented in the surface of fibronectin-coated of PAA hydrogels (no significant differences on gels stiffness was observed upon bead indentation, controlled with AFM). Labelled NC explants were placed 2 to 3 diameters in front of the beads and migration was registered by time-lapse.

Dispersion assay—As a read-out of EMT we used a cell dispersion assay on PAA hydrogels of varying stiffness. In brief, labelled neural crests were explanted into fibronectin-coated hydrogels and allowed to disperse. Dispersion was recorded by time-lapse.

Immunostaining and Phalloidin staining

For phospho-Myosin (ab2480, Abcam) and fibronectin (mAb 4H2 anti-FN, kindly provided by Dr Douglas DeSimone) immunostaining in flat-mounted embryos, whole animals were fixed using 2% TCA (trichloroacetic acid) in 0.3% PBS-T (PBS+0.3% Triton X-100) for 20-min. Dorsal halves of fixed embryos were dissected using a 15° 5-mm depth microsurgical knife (MSP 7516). Dissected halves were washed with PBS and blocked during 4 hours with 10% normal goat serum (NGS). Antibodies were diluted at 1:100 (ab2480) and 1:500 (anti-FN) in 10% NGS and incubated overnight (ON) at 4°C, followed by 3 washes with PBS-T. Alexa-fluor® (Thermo-Fisher) secondary antibodies were diluted 1:350 in 10% NGS and

incubated ON at 4°C, excess of antibody was removed by washing 3 times with PBS-T. Nuclei were stained with DAPI, DAPI was mixed with the secondary antibodies (1:1000). Finally, embryos were washed ON in MEOH and flat-mounted for imaging on clearing mix BA:BB (2 volumes benzyl alcohol and 1 volume benzyl benzoate, Sigma-Aldrich). For E-cadherin and N-cadherin detection, explants were fixed with 4% formaldehyde in 0.2% PBS-T (PBS+0.2% Triton X-100) for 12-min and blocked with 10% NGS for 2 hours. The primary antibody (anti-E-cadherin 5D3 or anti-N-cadherin MNCD2 Developmental Studies Hybridoma Bank) was diluted at 1:100 in 10% NGS and incubated ON at 4°C. Explants were washed 3 times with PBS+0.2% Tween-20 and incubated ON at 4°C with secondary antibody, diluted at 1:350 in 10% NGS. DAPI was diluted at 1:1000 and mixed with the secondary antibodies. To detect fibronectin on gels, functionalised gels were washed twice with PBS and incubated for 1 hour at room temperature with anti-Human fibronectin (Sigma S3648) diluted 1:500 in PBS. Gels were washed three times with PBS and incubated for 1 hour at room temperature with 1:350 Alexa-fluor® anti-Rabbit 488 + 1:1000 of DAPI. Gels were washed three times with PBS and maintained in 1% formaldehyde in PBS. Fluorescence intensity, was analysed using the measurement tool from ImageJ.

Phalloidin (A12379) stain was as follow: embryos where fixed in a mix containing 4%PFA/ 0.25%Glutaraldehyde for 10 min, washed 3 times in PBS-0.3% Triton-x100 for 10 min and incubated in a solution containing 5U of phalloidin per ml of PBS. Excess of Phallodin was washed with PBS-0.3% Triton-x100 and embryos were dehydrated in Isopropanol (10 min) and cleared and mounted on BB:BA 2:1 (Sigma).

Microscopy and time-lapse live-imaging

Time-lapse—Images for chemotaxis and dispersion assays (on gels and glass) were acquired every 5-min at 18°C using an upright microscope (DMR XA2, Leica) equipped with a motorized stage (Prior Scientific), and a camera (Orca-5G Hamamatsu). Filter wheels, camera, stage, and shutters were controlled with SimplePCI software (Hamamatsu). A 20x objective (HCX APO L 20x/0.50 W U-V-I FWD= 3.50 mm, Leica) was used.

Confocal time-lapse—Images were acquired every 16-sec at 18°C using an upright confocal integrated microscope system (SP8vis, Leica) with a 63x objective (HCX APO L 63x/0.90 W U-V-I CS2, FWD= 2.20 mm, Leica).

Live-imaging—For graft experiments, time-lapse images were acquired every 10-min with an upright microscope (Eclipse 80i; Nikon) fitted with a motorized stage (Prior Scientific) and a camera (ORCA-05G; Hamamatsu Photonics). Images were acquired at 18°C with a 4x objective (CFI Plan Fluor 4x/0.13, WFD= 17.1 mm). Camera, stage, shutter and filter wheels were controlled with a SimplePCI software (Hamamatsu).

In situ hybridization imaging—All images were captured at room temperature in agarose dishes filled with PBS, using a dissecting microscope (MZ FL III; Leica) equipped with a camera (DFL420; Leica) and an imaging software (IM50, Leica). Magnification was 3.2x.

Immunofluorescence imaging—All images were acquired at room temperature. Images in Fig. 3 a, b, j, k; Extended Data Fig. 2b,f; Extended Data Fig. 4d,g; Extended Data Fig. 6; Extended Data Fig. 6; and Extended Data Fig. 9f,e were acquired in an inverted confocal microscope (FluoView FV1000; Olympus), equipped with a digital camera (DP73; Olympus) and a 20x objective (UPLSAPO 20X/0.75 FWD= 0.6 mm, Olympus). Camera, filter wheels, and shutters were controlled by FluoView Software (Olympus). Confocal images in Extended Data Fig. 2k and Extended Data Fig. 3 were acquired using an upright confocal integrated microscope system (SP8vis, Leica) with a 63x objective (HC PL APO 63x/1.40 Oil CS2, FWD= 0.14 mm, Leica).

In vivo atomic force microscopy measurements (iAFM)

All AFM measurements were carried out as previously described[12,21,25,40]. In brief, a JPK Nanowizard Cellhesion 200 (JPK Instruments AG), fitted with a x/y-motorized stage and mounted on an inverted optical microscope (Axio ObserverA1, Zeiss) was used. Customized cantilevers were used. For mesoderm AFM measurements, tipless silicon cantilevers (Arrow-TL1; NanoWorld) were mounted on the AFM device and spring constant were calculated by the thermal noise method[39]. Cantilevers with spring constants between 0.01 and 0.03 N/m were selected. Monodisperse polystyrene beads (diameter: 37.28 ± 0.34 μm; microParticles GmbH) were glued to the selected cantilevers[12,21,25]. Embryos where mounted on a clay modelling dish and the epidermis was carefully dissected using a hair knife. Force–distance curves were acquired every 15 μm in the region which is immediately lateral to the NC, as shown in Fig. 1g and Extended Data Fig. 3a. A region of interest was defined using a custom-written script that controls the x/y-motorized stage (maximum indentation force: 7 nN, approach speed: 5 μm/s, data rate: 1,000 Hz). Measurements on intact embryos were carried out in the same territory, but embryos were not dissected. In these experiments, monodisperse polystyrene beads (diameter: 89.3 ± 1.1 μm; microParticles GmbH) were glued to tipless silicon cantilevers with spring constants of ~0.1 N/m (Shocon-TL; AppNano, CA, USA), and force–distance curves were acquired with a maximum indentation force of 50 nN, approach speed: 5 μm/s, data rate: 1,000 Hz, one measurement per embryo. For extrinsic compression experiments, stress was applied in the same region were measurements were taken (Fig. 2m) with 89.3 ± 1.1 μm beads as cantilever probes. A sustained force of 80 nN (Control embryos) and 50 nN (DshDEP[+] injected embryos) was applied to compress the tissue. Force was applied until embryos reached pre-migratory (Control and DshDEP[+]) or migratory stages (DshDEP[+]). Uncompressed time-matched embryos and the contralateral side of the compressed embryo were used as controls. An image was acquired for each measurement, using an adapted AxioZoom V.16 system (Zeiss) connected to an Andor Zyla 4.2 CMOS camera. After compression, embryos were rapidly fixed for in situ hybridization. Displacement maps were generated using the ImageJ iterative PIV basic plugin.

Data analysis and image treatment

AFM data—Force–distance curves were analysed as previously described, using a customized Matlab routine based on the Hertz model for a spherical indenter[12,21,25]:

$$F = \frac{4}{3}K\sqrt{r}\delta^{3/2} = \frac{4}{3}\frac{E}{1-v^2}\sqrt{r}\delta^{3/2}$$

With applied force F, Young's modulus E, Poisson's ratio v, indenter radius r, indentation depth δ, and apparent elastic modulus $K = E/(1 - v^2)$ referred as 'Apparent Elasticity' in the text. Force–distance curves from the measurements taken in the region of interest were analysed for defined indentation depths of 3μm, which has been shown to measure mechanical properties of developing tissues[12,21,25,40]. Averages of maximum indentation depth are included in each figure. Measurements for each experiment were pooled and statistically analysed. Representative examples of force curves with highlighted indentation depths (δ) are provided (Extended Data Fig 2i,j). Average indentation depth (δ) for each AFM experiment is included below the corresponding charts.

In vivo analysis of NC migration—For in situ hybridised embryos, the length of the treated NC was normalised against the length of the contralateral control side of the embryo. For grafted embryos, the length of the NC was normalised versus the total dorsoventral length of the embryo at the position of the NC. Lengths were obtained using the measurement tool from ImageJ and further analysed as described in statistical analysis methods.

Ex vivo analysis of NC migration—Manual tracking and chemotaxis tool plugins from ImageJ were used to calculate speeds of migration. For dispersion assays, an ImageJ -based custom-made Delaunay triangulation plugin[13] was used to calculate the distance between neighbour cells (available upon request). Data was further analysed as described in statistical methods section.

Cell density measurements—Confocal images of transverse sections stained for DAPI were projected on ImageJ. A region of interest (RoI) was selected in the mesoderm under the NC in embryos at non-migratory stages, nuclei number within this region was quantified and nuclei density calculated as the number of nuclei within the RoI divided by the area of the RoI. The same RoI size was used to calculate density at st17 and pre-migratory stages. Cell density was expressed in nuclei per square micron.

Image treatment—Z-stacks, maximum projections and time-lapse movies were created using ImageJ software. Adjustment of display map levels, re-sizing, addition of scale-bars, and pseudo-colour were applied with ImageJ and/or Photoshop (Adobe). In Figure 2 c, g, h, k, o, Figure 3a (pre-migratory in situ hybridization panel) and Figure 4b, the background was pseudo-coloured. Pseudo-colour was done in Photoshop (Adobe).

Cryo-sectioning

Fixed embryos were washed twice for 5-min with PB buffer (phosphate buffer; 0.2 M NaH2PO4*H2O and 0.2 M K2HPO4, pH 7.4), incubated for 2 hours at RT with a solution containing 15% sucrose (Sigma-Aldrich) in PB (w/v) and 1 hour at 42°C in a gelatin solution, containing 8% gelatin (Sigma-Aldrich), 15% sucrose in PB (w/v). Embryos were

oriented in gelatin solution and gelatin blocks containing the embryos were snap frozen at -80°C with pre-chilled Isopentane. Samples were sectioned in 20 μm slices using a cryostat (CM-3050S, Leica) and collected in SuperFrozen® Slides (VWR International). The slides were dried for at least 6 hours and the gelatin was removed by washing twice with PBS for 15-min. MOWIOL (EMD Millipore) was used as mounting media.

Statistical analysis

Sample size was determined by following literature in the field and no statistical method was used. Due to the nature of the experiments performed along this work, the authors were not blinded to allocation during experiments and results analysis, just viable embryos and cell clusters were included for analysis in this study. Additionally, miss-injected embryos were excluded from *in situ* hybridisation analysis (correct injection was monitored by co-injection of linear tracing molecules mRFP or FDX). After selecting surviving and properly injected embryos and/or cells, our parameters for different experiments were measure at random.

Each experiment was repeated at least three times. Normality was tested for the spread of data of each experiment using KolmogorovSmirnov's test, d'Agostino and Pearson's test, or ShapiroWilk's test in Prism7 (GraphPad). Significances for data sets displaying normal distributions were calculated in Prism7 with an unpaired Student's t-test (two-tailed, unequal variances) or one-way analysis of variance (ANOVA) for multiple comparisons. Individual comparisons were calculated just when ANOVA was $p<0.05$. Significances for non-normal distributed data were calculated in Prism7 using Mann-Whitney's test. Meaning for boxes, histograms, error bars and whiskers are explained in the legend of each figure.
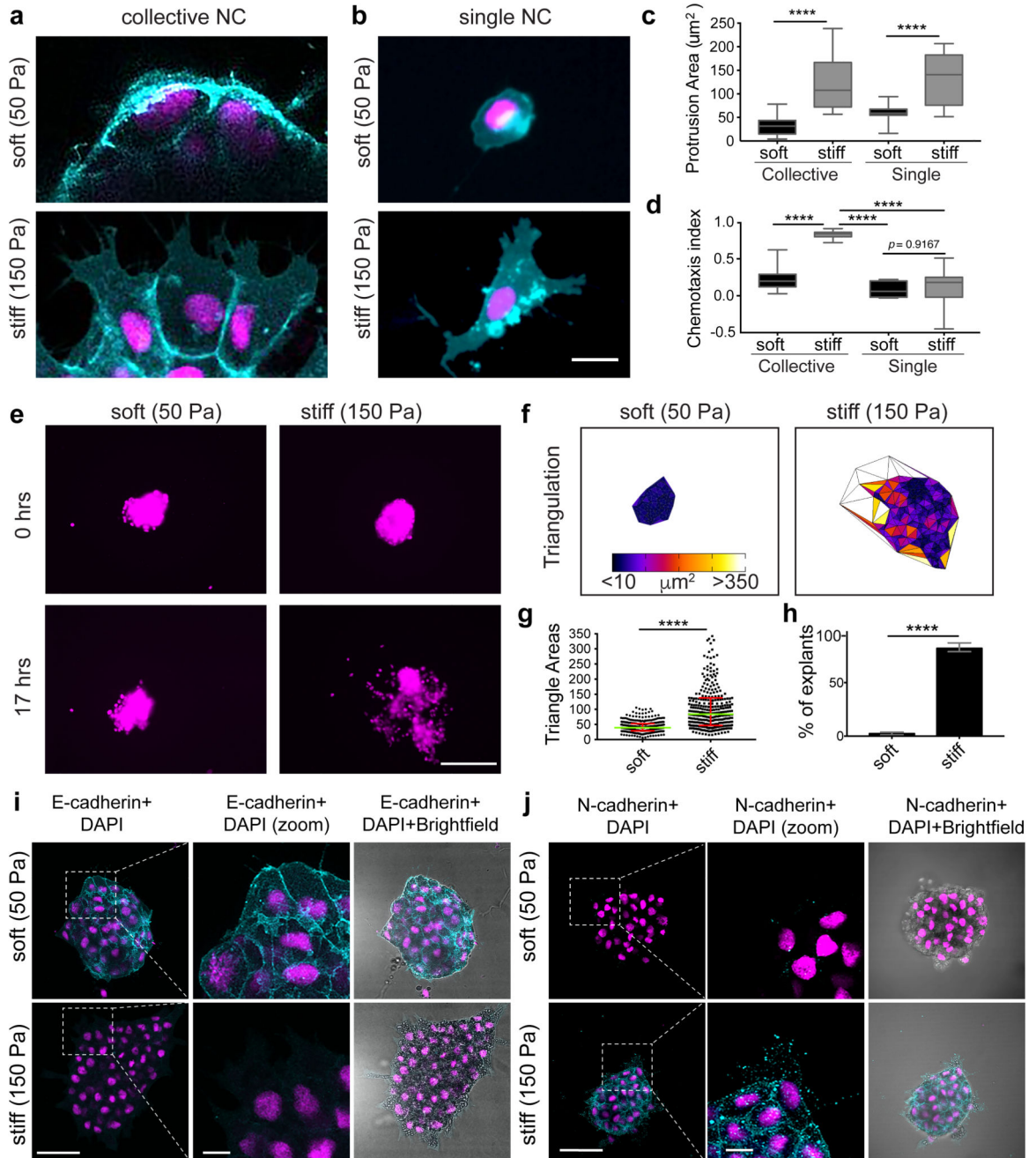
Extended Data
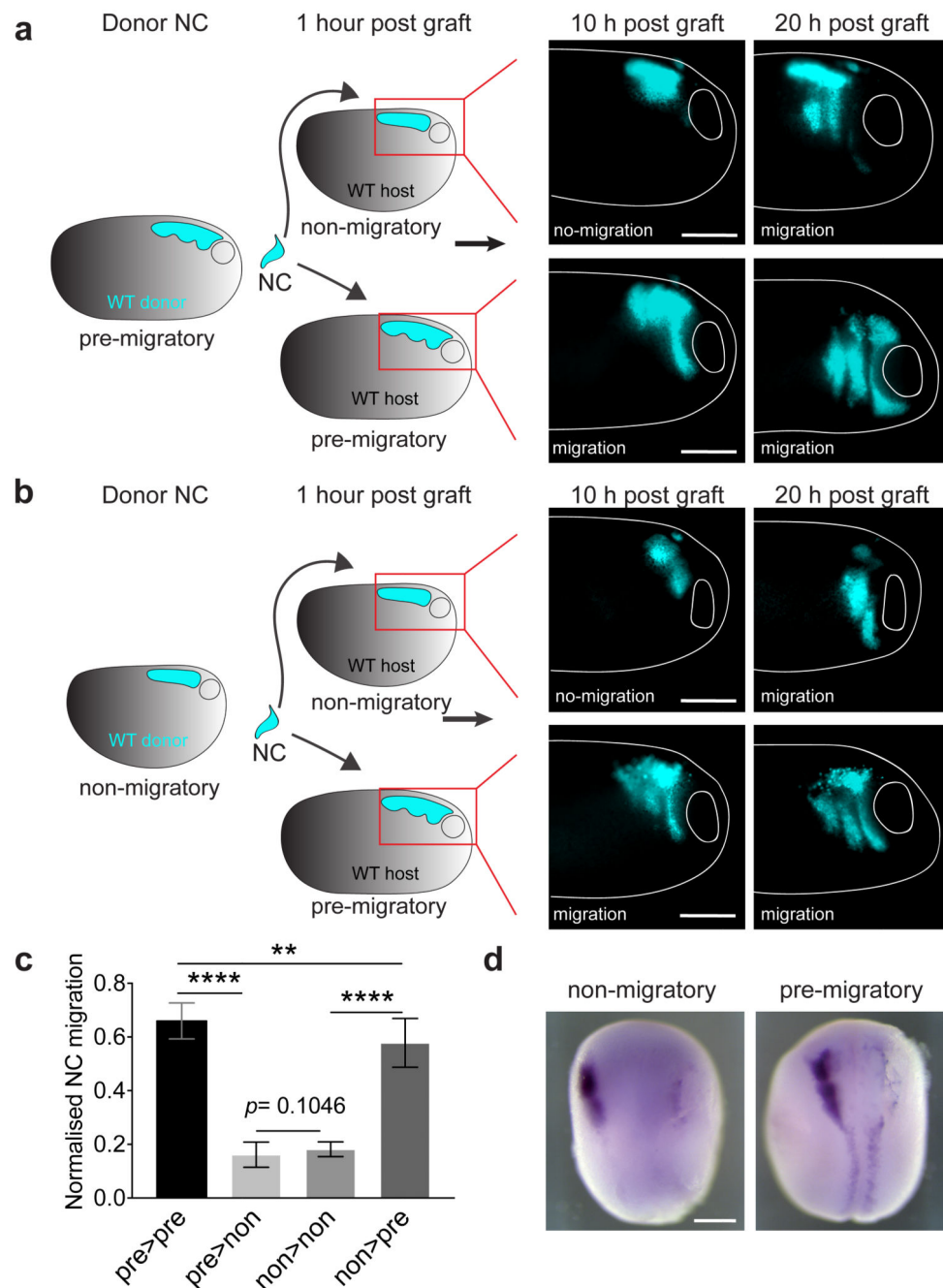
Extended Data Figure 1. Neural crest migration is controlled by environmental factors.
(a–d) Heterochronic graft controls. In all grafts, we completely removed the host NC prior
to implanting the graft, and all grafted cells migrated 20 hours post graft, as expected for
embryos reaching the migratory stage (stage 23)7. **(a)** Labelled pre-migratory NC grafted
into unlabelled non- and pre-migratory hosts. 10 hrs post graft, representative examples
showing that pre-migratory NC grafted into non-migratory hosts is not migrating and that

pre-migratory NC grafted into pre-migratory hosts does migrate. **(b)** Labelled non-migratory NC grafted into unlabelled non- and pre-migratory hosts. 10 hours post graft, representative examples showing that non-migratory NC grafted into non-migratory hosts are not migrating and that pre-migratory NC grafted into pre-migratory hosts does migrate. 20 hours post graft panels in **a, b** show that NC migrated in all conditions after 20 hours. **(c)** Normalised NC migration, histograms represent media, error bars SD, N= 80 measurements from 20 embryos (one-way ANOVA P <0.0001, two-tailed *t*-test **P=0.0026, ****P<0.0001, CI= 95%). **(d)** Dorsal views of embryos hybridised with a probe against *snail2* after dissection of the host NC, showing that endogenous NC was completely removed prior to graft. **a,b,d** representative examples of three independent experiments, scale bar 250 μm. NC, neural crest.
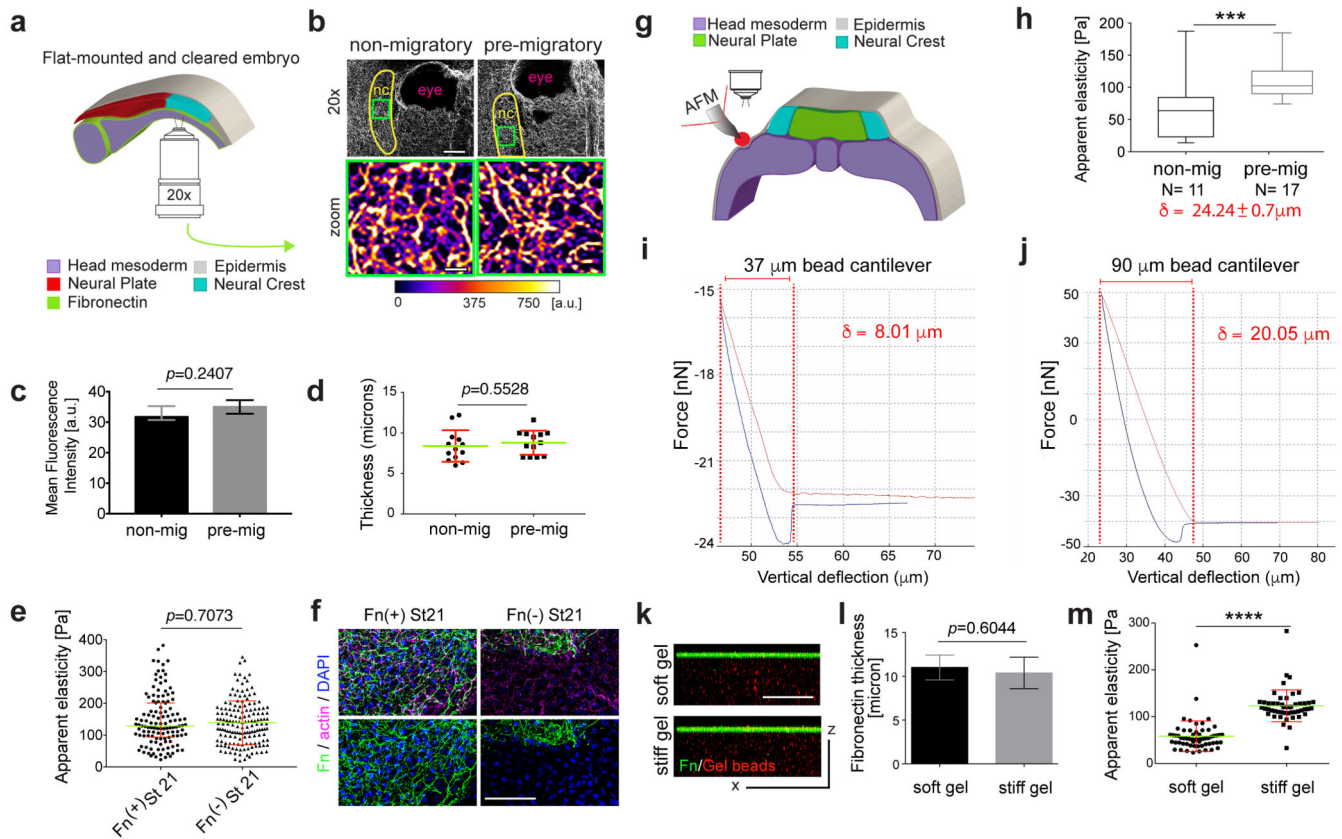
Extended Data Figure 2. Fibronectin expression under the neural crest *in vivo* and contribution to tissue stiffness, stiffness measurements across epidermis, and *ex vivo* system characterisation. **(a–d)** Analysis of Fibronectin expression under the NC. **(a)** Schematic showing the imaging method used to access Fibronectin under the NC. **(b)** Immunostaining for Fibronectin on embryos at non- and pre-migratory stages. 20x panels, yellow outline is highlighting the anatomical position of the NC, green box highlights the region showed in the zoom panels. Zoom panels show heat maps of Fibronectin signal (representative of 5 independent samples). **(c)** Fluorescence signal intensity, histogram represents media and error bars SD (two-tailed *t*-test, CI= 95%). **(d)** Fibronectin signal thickness in the mesoderm at pre- and non-migratory stages, green lines represent media and red whiskers SD; N_c= 10 animals,

N_d= 26 sections from 3 independent experiments (two-tailed t-test, CI= 95%). Scale bars (20x panels) 50 µm, (zoom panels) 20 µm. NC, neural crest. **(e–f)** Apparent elasticity was measured before and after mechanical removal of the ECM by gently scraping the surface of the tissue with a hair loop. **(e)** Apparent elasticity was measured directly on the mesoderm in the presence Fn(+) or absence Fn(-) of Fibronectin (Fn, green) in embryos at stage 21 (pre migratory). Spread of data is plotted, green lines represent median, red whiskers interquartile range (two-tailed Mann–Whitney, ***P<0.0006, CI= 95%, n= number of AFM-indentations, $n_{fn}^{(+)}$= 124, $n_{fn}^{(-)}$= 157). Average indentation depth= 8µm. **(f)** Immunostaining against Fibronectin (Fn), conditions as indicated. two-tailed Mann Whitney test, p value as indicated, N= 7 embryos. Scale bar 100 µm. **(g–h)** AFM controls. **(g)** Schematic of iAFM measurement. To control that the dissection of the epidermis did not modify the mesodermal elasticity we measured the elastic moduli through the epidermis and no differences were observed (compare with Fig. 1h). **(h)** Apparent elasticity, boxes show the 25th, median, and 75th percentiles; whiskers show the spread of data (excluding outliers) (two-tailed Mann–Whitney, ***P=0.0006, CI= 95%, N= number of animals δ= average indentation depth). **(i–j)** Representative examples of force curves obtained from measurements performed using cantilevers coated with either **(i)** 37 µm beads, n_i= 2386 or **(j)** 90 µm beads, n_j= 28; (red lines represent cantilever extension and dark blue lines retraction). Indentation depth (δ) for each curve is provided. **(k–m)** *ex vivo* system characterization. **(k)** Cross-sectional confocal image of stiff or soft PAA hydrogels, confirming that gels (red) of varying stiffness values are evenly functionalized with Fibronectin (green). **(l)** Fibronectin thickness does not change between soft and stiff gels, N= 8 gels (two-tailed t-test, CI= 95%). Results in **k** and **l** are representative gels from three independent experiments. **(m)** AFM measurements, spread of data, green lines represent median, red whiskers interquartile range (two-tailed Mann–Whitney, ***P<0.00060, CI= 95%, n_{stiff}= 60, n_{soft}= 50 from 10 gels). Scale bars **(k)** 50 µm.

Extended Data Figure 3. Neural crest motility, dispersion, and EMT are controlled by substrate mechanics.

(a–d) Protrusion and chemotaxis analysis of collective and single NC cells plated on soft and stiff substrates. **(a)** Confocal projections of labelled NC collectives plated on soft or stiff gels. **(b)** Confocal projections of labelled single NC cells plated on soft or stiff gels. **(c)** Protrusion area and **(d)** chemotaxis quantifications for collective and single NC cells plated on soft or stiff gels, boxes show the 25th, median, and 75th percentiles; whiskers show the spread of data (excluding outliers) $N_{protrusion\_area}$= 63 cells, $N_{chemotaxis}$= 79 cells (one-way

ANOVA P <0.0001, two-tailed *t*-test ****P<0.0001, CI= 95%). (e–h) NC dispersion analysis on gels of varying stiffness. (e) NC cells labelled with nRFP and plated on stiff or soft gels are shown at 0 and 17 hours after plating. (f–h) quantification of cell dispersion. (f) Color-coded Delaunay triangulation shown at 17 hours after plating to facilitate visualization of the distances between neighbor cells. (g) Quantification of Delaunay triangulation, spread of data for each condition is plotted, green lines represent median, red whiskers the interquartile range (two-tailed Mann–Whitney, ****P<0.0001, CI= 95%, N_g= 730 triangles from 31 explants. (h) percentage of dispersing explants, histograms represent media and error bars s.e.m. (two-tailed *t*-test ****P<0.0001, CI= 95%, N_h= 31 explants) g and h, are data from 4 independent experiments (soft) and 3 independent experiments (stiff). (I,j) Immunostaining for (i) E-cadherin and (j) N-cadherin on NC plated on substrates of varying stiffnesses. a–b,e,i,j representative examples of 3 independent experiments. Scale bars (a,b) 20 μm, (e) 250 μm, (I,j) 50 μm, (I,j, zoom) 10 μm.
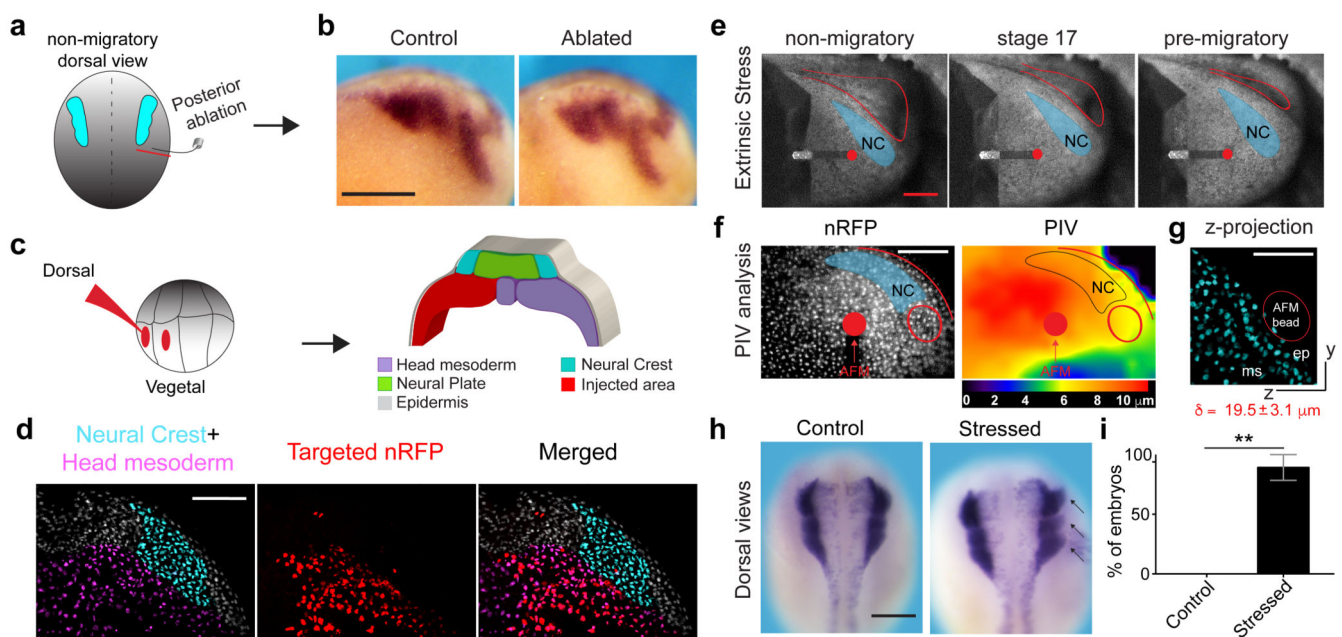
Extended Data Figure 4. Posterior ablations, mesoderm targeted injections, and extrinsic compression characterisation.
(a–b) Ablation controls. Mechanical tension in *Xenopus* is higher in the anterior region of the embryo than in posterior territories12,41. Consistent with this observation, no effect on NC migration or tissue stiffness was observed when the ablation was done in posterior regions. (a) Schematic showing embryos ablated at non-migratory stages, and NC migration at stage 23 (migratory)7. (b) Lateral views of Control and posteriorly ablated embryos hybridised with a probe against *snail2*. (c–d) Targeted injections to the head mesoderm. (c) Cartoon shows that injecting 2 dorso-vegetal blastomeres targets the head mesoderm. (d) Confocal images of targeted injections showing nuclear RFP expression in the mesoderm, panels as labelled in the figure. Scale bars (b) 250 μm, (d) 100 μm. (e–g) Compression controls. (e) Images of embryos being compressed from non- to pre-migratory stages with a 90-micron diameter bead attached to an AFM cantilever (bead, red circumference), neural

plate border highlighted with red lines and NC position shown in light-blue, stages as labelled. **(f)** Magnitude maps from a particle image velocity (PIV) analysis indicates the x/y extent of the deformation induced by AFM indentation. **(g)** Maximum projection of a cross-section showing the z-deformation generated by the AFM compression, epidermis (ep) and mesoderm (ms) are being deformed, averaged maximum indentation depth (δ) is provided (nuclei are visible in the bead region due to a maximum projection effect). **(h,i)** Result of extrinsic stress experiments. **(h)** Dorsal view (anterior to top) of embryos hybridised with a probe against *snail2*, black arrows point to migrating NC. **(i)** Percentage of embryos displaying NC migration, histograms represent media, error bars s.e.m. N= 13 animals (two-tailed *t*-test **P=0.0010, CI= 95%). All experiments repeated three times. Scale bars **(e, f)** 200 μm, **(g)** 100 μm, **(h)** 200 μm.
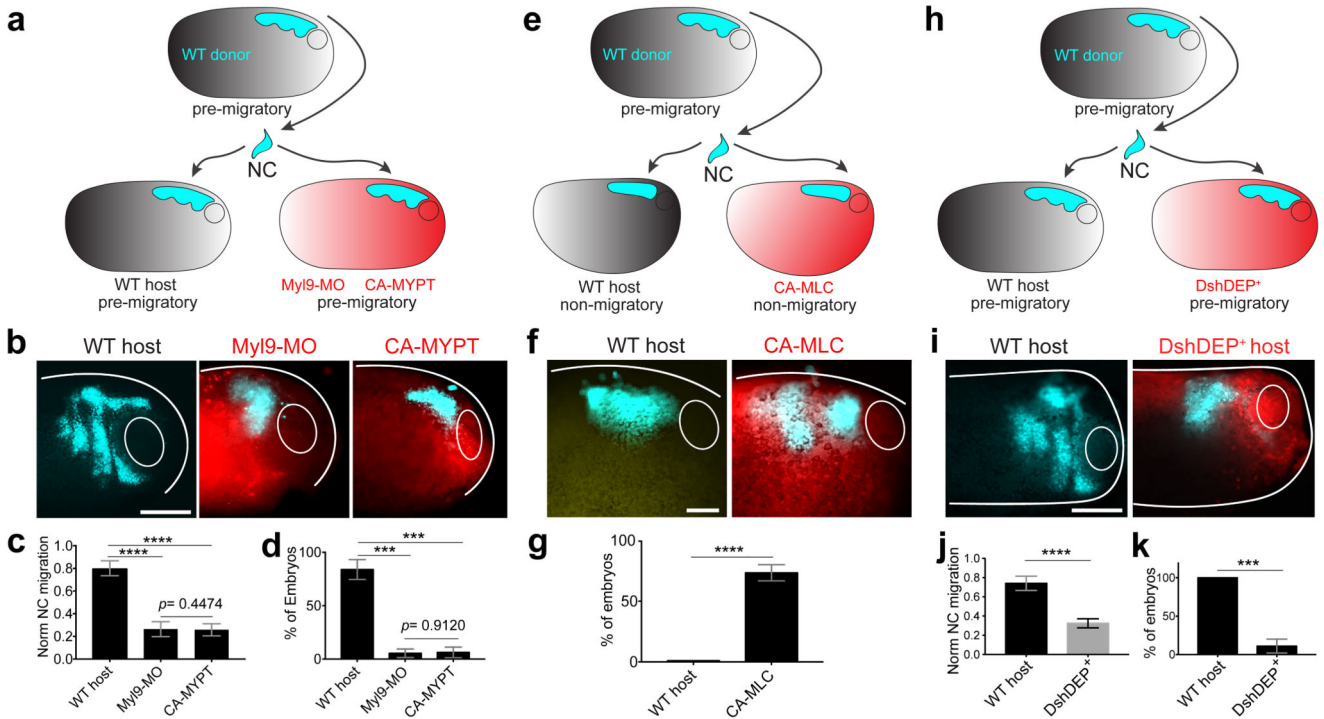
Extended Data Figure 5. Mesodermal stiffening promotes neural crest collective migration in a non-autonomous manner *in vivo*.

(a–d) Non-autonomous effect of mesodermal myosin manipulations on NC migration *in vivo*. **(a)** Wild type labelled pre-migratory NC (cyan) grafted into pre-migratory wild type (WT), Myl9-MO, or CA-MYPT injected hosts (mesoderm in red). **(b)** Representative embryos showing normal NC migration in WT hosts and inhibited NC migration in Myl9-MO or CA-MYPT hosts. **(c)** Normalised NC migration N= 22 animals and **(d)** percentage of embryos displaying NC migration (one-way ANOVA P <0.0001; two-tailed *t*-test ***P<0.0006, ****P<0.0001, CI= 95%, N= 38 animals). Histograms in **c, d, g** represent media, error bars in **c** SD or s.e.m in **d,g**. **(e–g)** Effect of premature mesodermal stiffening on NC migration *in vivo*. **(e)** Wild type labelled pre-migratory NC grafted into non-migratory wild type (WT), or CA-MLC hosts. **(f)** Representative embryos showing premature NC migration in CA-MLC hosts, while no migration is observed in control embryos at this

stage. **(g)** Percentage of embryos displaying NC migration, two-tailed t-test ****P<0.0001, CI= 95%, N= 20 animals. **(h-k)** Non-autonomous effect of DshDEP+ on NC migration. **(h)** Wild type labelled pre-migratory NC (cyan) was grafted into pre-migratory wild type (WT), or DshDEP+ hosts. **(i)** Representative examples showing NC migration in WT hosts and inhibited NC migration on DshDEP+ injected hosts (mesoderm in red). **(j)** Normalised NC migration and **(k)** percentage of embryos displaying NC migration (two-tailed *t*-test ***P<0.0002 ****P<0.0001, CI= 95% N= 14 animals). Histograms in **j, k** represent media and error bars **(j)** s.e.m and **(d)** SD. **b,f,i** are representative examples of 3 independent experiments. Scale bars **(b)** 200 μm, **(f)** 100 μm, **(i)** 150 μm.
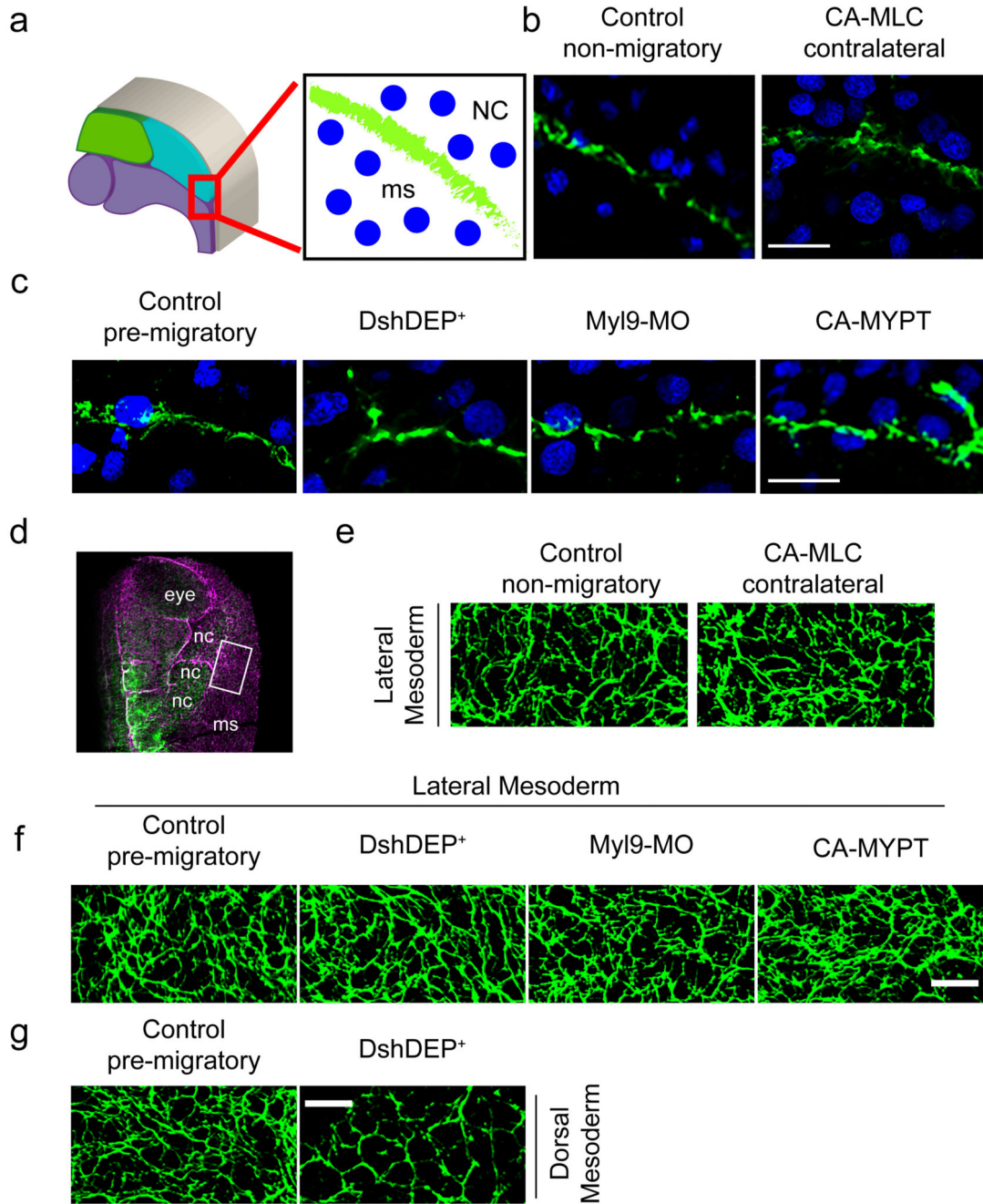
Extended Data Figure 6. Head mesoderm manipulations did not affect Fibronectin deposition and organization under the NC.

As it has been previously described that myosin and PCP inhibition can affect Fibronectin deposition and organization in dorsal mesoderm27,28,42; we analyse the effect of these treatment in the lateral mesoderm underlying the premigratory NC. Our results show no effect of myosin or PCP inhibition in Fibronectin deposition or organization in lateral mesoderm, indicating that the effect of our treatments on NC migration are not due to an indirect effect on Fibronectin, but rather a consequence of affecting mesoderm stiffness. (**a–**

c) Transverse sections showing Fibronectin expression under different treatments used to manipulate head mesoderm's apparent elasticity. **(a)** Schematic showing the area presented in **b–c**. **(b–c)** Immunostaining against Fibronectin (green) and DAPI stain (blue) showing Fibronectin signal underneath the NC, treatments as labelled in each panel. Scale bar 30 μm. **(d–g)** Effect of mesoderm manipulation on Fibronectin assembly. **(d)** Dorsal view of a flat-mounted embryo, white square indicates the area shown in b and c. **(e)** Immunostaining against Fibronectin (green) in non-migratory embryos (stage 13), showing Fibronectin assembly underneath the NC, treatments as indicated. **(f)** Immunostaining against Fibronectin (green) in pre-migratory embryos (stage 20) showing Fibronectin assembly underneath the NC, treatments as indicated. **(g)** Control to show that inhibition of PCP signaling (DshDEP[+]) affects Fibronectin assembly of dorsal mesoderm42, but not in lateral mesoderm **(f)**. Scale bars 30 μm. **b–c** and **e–g** are representative examples of 3 independent experiments.
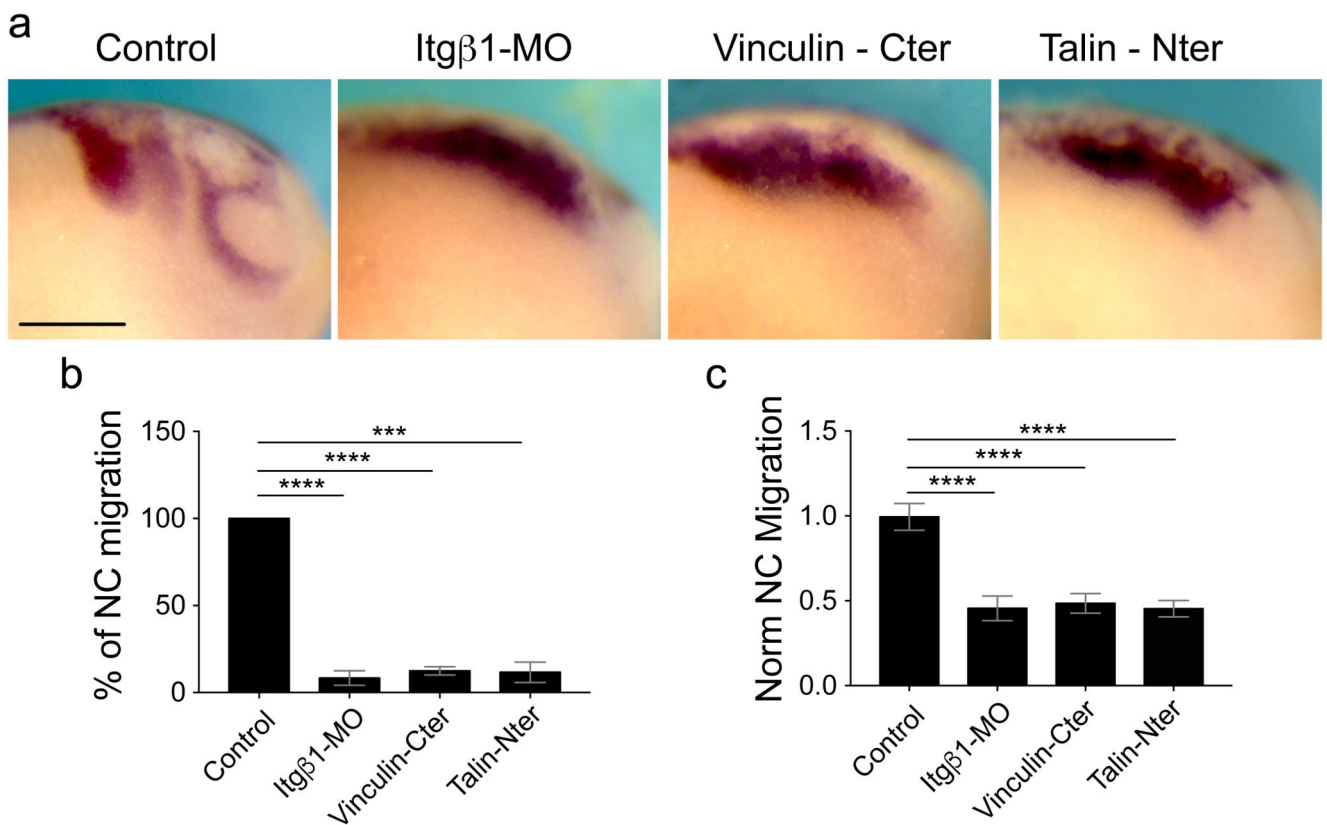
Extended Data Figure 7. NC senses mesoderm stiffening by using an Integrin/Vinculin/Talin-mediated mechanoresponsive mechanism.
**(a–c)** Analysis of NC migration after Integrin-β1, Vinculin or Talin knockdown. **(a)** Lateral views of embryos hybridised with a probe against *snail2*. Control embryos migrate normally from dorsal to ventral. However, NC migration is drastically inhibited in embryos treated with Itgβ1-MO or the negative dominants Vinculin-Cter or Talin-Nter. Embryos in **a** are representative examples of 3 independent experiments. **(b–c)** quantification of neural crest migration showing **(b)** percentage of embryos and **(c)** normalised NC migrated distances.

Histograms represent media, error bars SD. (one-way ANOVA P <0.0001, two-tailed *t*-test ***P<0.0002 ****P<0.0001, CI= 95%). N= 39 embryos. Scale bar 200 μm.
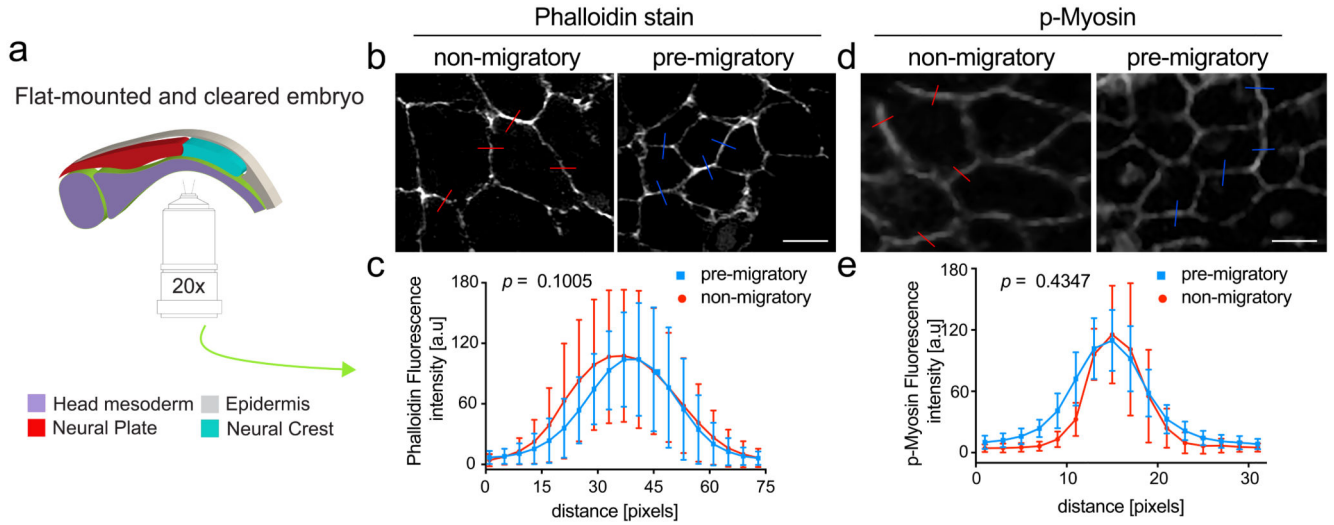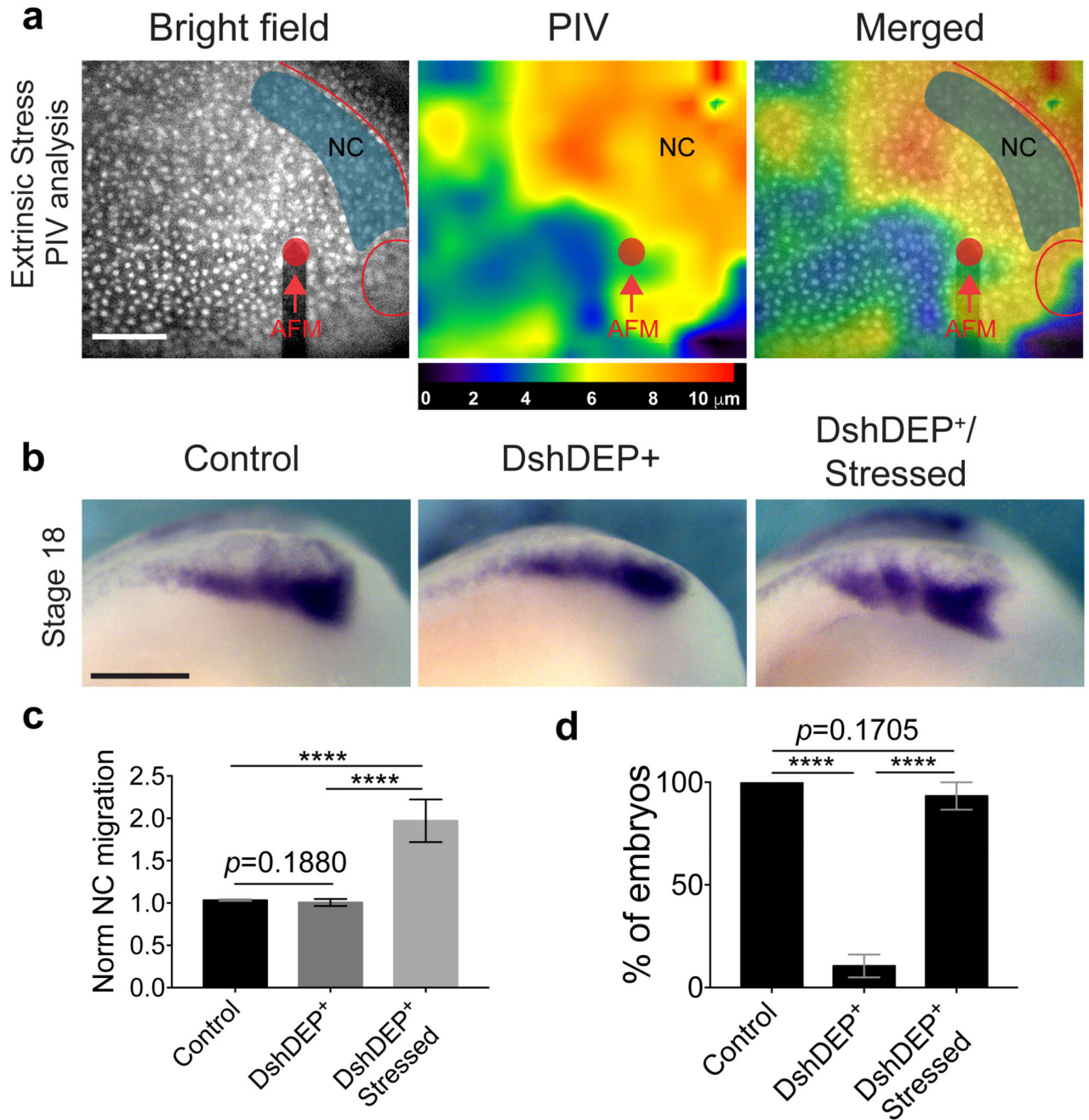

Extended Data Figure 8. Actomyosin expression in the head mesoderm does not change from non- to pre-migratory stages.

(a–e) Analysis of actin and phospho-myosin expression under the NC. As actomyosin contractility has been proposed to contribute to paraxial mesoderm stiffness in Xenopus13, we assessed actomyosin activity in the head mesoderm, the substrate of the NC. Note that the expression levels of either actin or p-myosin remained unchanged at pre-migratory stages compared to non-migratory stages. **(a)** Schematic showing the imaging method used to access the head mesoderm under the NC. **(b)** Phalloidin stain was used to label actin on embryos at non- and pre-migratory stages. **(d)** Immunostaining against phospho-myosin on embryos at non- and pre-migratory stages. **(c–e)** quantification of fluorescence intensity across the membrane represented by a continuous line, each point represents media and error bars SD; n, number of measurements per data (time) point, n_c= 16, n_e= 15, from 3 independent experiments, non-significant differences were observed, *p* value is indicated in each chart (two-tailed *t*-test, CI= 95%). Scale bars 20 μm.
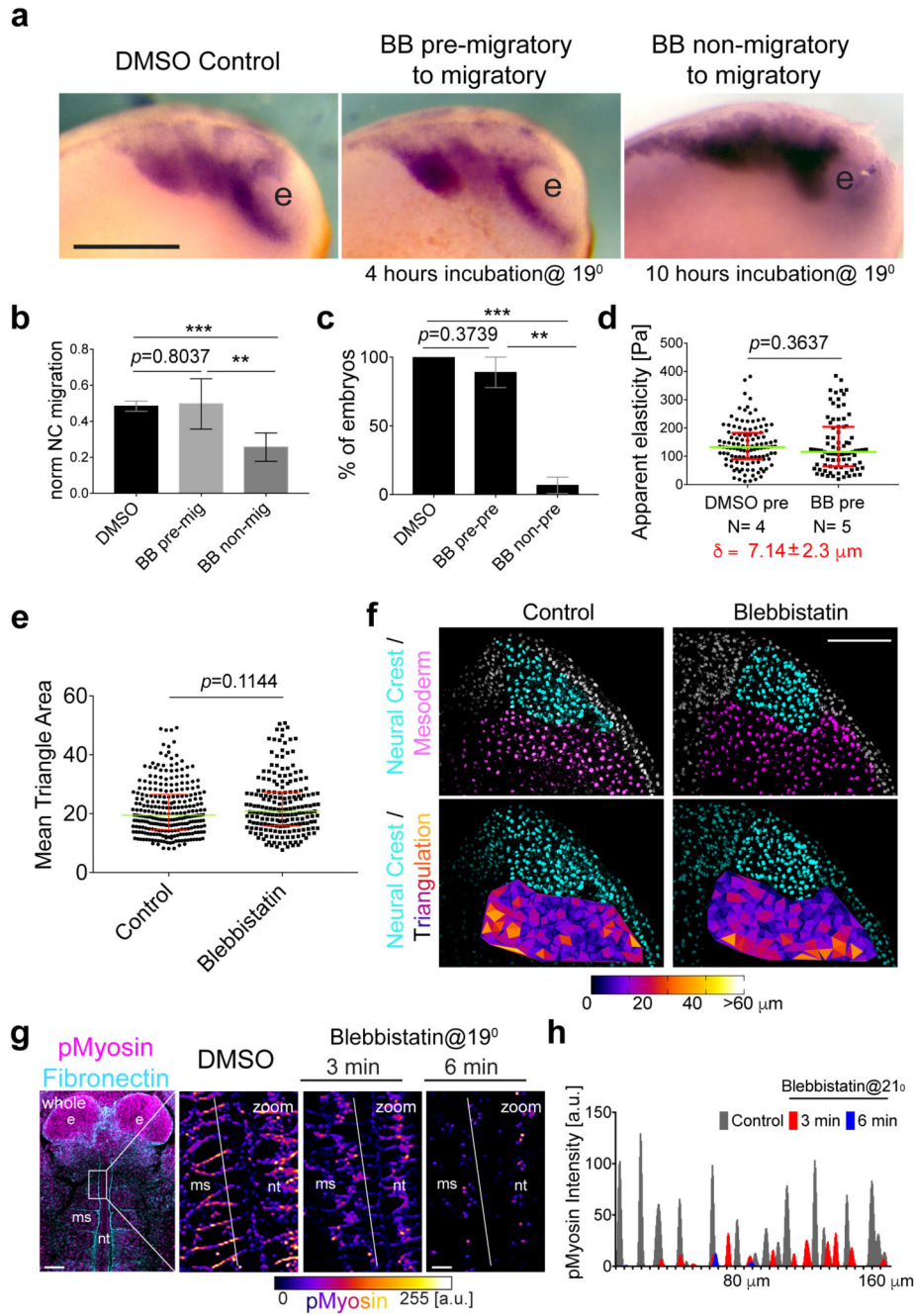
Extended Data Figure 9. Myosin contractility is not required to maintain mesodermal stiffness.
(a–f) Blebbistatin incubation experiments. To functionally test the effect of actomyosin contractility on mesoderm stiffness, we applied blebbistatin on pre-migratory embryos. Note that blebbistatin treatment at this stage did not affected mesoderm stiffness, cell density or NC migration, in spite of a dramatic reduction in myosin phosphorylation. **(a)** Lateral views of embryos hybridised with a probe against *snail2*, showing no differences in NC migration after 4 hours of incubation with DMSO or Blebbistatin (BB), embryos were incubated as indicated. **(b)** Normalised NC migration and **(c)** percentage of embryos. Histograms and

error bars on **c, d** represent medians and SD respectively (one-way ANOVA P <0.0001, two-tailed *t*-test **P<0.008, ***P<0.002, CI= 95%, N= 19 animals). **(d)** iAFM measurement direct on mesoderm; Spread of data plotted for each condition, green lines represent median, red whiskers the interquartile range (two-tailed Mann–Whitney test, p value as indicated, CI= 95%, n= number of AFM-indentations, n_{DMSO}= 116, n_{BB_pre}= 204, N= number of animals, δ= averaged maximum indentation depth). **(e–f)** As blebbistatin treatment could affect cell-cell adhesion promoting cell dispersion, we measured its effect on cell dispersion by calculating the distance between neighbor mesoderm cells. **(e)** Chart comparing the mean area of the triangle formed by each mesoderm cell with its neighbours, calculated by Delaunay triangulation (Mann Whitney test p value as shown). **(f)** Images showing neural crest and mesoderm cells (treated as indicated) and triangles from which the areas were calculated. Scale bar 200 μm **(g)** Immunostaining for phospho-Myosin (pMyosin), dorsal view of a flat-mounted embryo and color-coded intensity of zoom images at the indicated time points are shown (scale in arbitrary units). **(h)** Fluorescence intensity in arbitrary units [a.u.] across the white line in the zoom panels. All experiments repeated at least three times. **a,f,g** are representative examples of 3 independent experiments. Scale bars **(b)** 150 μm, **(e,** whole**)** 100 μm, **(e,** zoom**)** 15 μm. ms, mesoderm; nt, notochord; e, eye.

a Bright field | PIV | Merged

Extrinsic Stress PIV analysis

NC — AFM

0 2 4 6 8 10 μm

b Control | DshDEP+ | DshDEP+/Stressed

Stage 18

c Norm NC migration

**** ****

p=0.1880

Control DshDEP+ DshDEP+ Stressed

d % of embryos

p=0.1705

**** ****

Control DshDEP+ DshDEP+ Stressed

Extended Data Figure 10. Extrinsic compression modifies the environment of PCP depleted embryos and triggers premature neural crest collective migration, *in vivo*.
(a), Magnitude maps from a particle image velocity (PIV) analysis presented to facilitate the visualisation of the x/y extent of the stress field generated by the extrinsic compression experiment (scale bar in microns). Neural plate border shown in red lines, neural crest in light blue. **(b–c)** Extrinsic stress-induced premature NC migration. (b) Lateral views of embryos hybridised with a probe against *snail2*, notice NC premature migration is observed in the DshDEP+/Stressed panel. **(c)** Normalised NC migration and **(d)** percentage of

embryos displaying each phenotype are shown. Histograms and bars represent media and SD, (one-way ANOVA P <0.0001, two-tailed t-test ****P<0.0001, CI= 95%, N= 18 animals). Images in a and b are representative examples of 3 independent experiments. Scale bars **(a)** 200 μm, **(b)** 150 μm.

Supplementary Material

Refer to Web version on PubMed Central for supplementary material.

Acknowledgements

References

1. Roca-Cusachs P, Sunyer R, Trepat X. Mechanical guidance of cell migration: lessons from chemotaxis. Current Opinion in Cell Biology. 2013; 25:543–549. [PubMed: 23726023]

2. Mayor R, Etienne-Manneville S. The front and rear of collective cell migration. Nature Reviews Molecular Cell Biology. 2016; 17:97–109. [PubMed: 26726037]

3. Kerosuo L, Bronner-Fraser M. What is bad in cancer is good in the embryo: Importance of EMT in neural crest development. Seminars in Cell & Developmental Biology. 2012; 23:320–332. [PubMed: 22430756]

4. Gilmour D, Rembold M, Leptin M. From morphogen to morphogenesis and back. Nature. 2017; 541:311–320. [PubMed: 28102269]

5. Nieto M, Huang R, Jackson R, Thiery J. EMT: 2016. Cell. 2016; 166:21–45. [PubMed: 27368099]

6. Betancur P, Bronner-Fraser M, Sauka-Spengler T. Assembling neural crest regulatory circuits into a gene regulatory network. Annual Review of Cell and Developmental Biology. 2010; 26:581–603.

7. Nieuwkoop, PD., Faber, J. "Normal table of *Xenopus laevis* (Daudin): A systematical and chronological survey of the development from the fertilized egg till the end of metamorphosis. Second edition. North-Holland Pub. Co.; Amsterdam: 1967. p. 260

8. Theveneau E, et al. Collective Chemotaxis Requires Contact-Dependent Cell Polarity. Developmental Cell. 2010; 19:39–53. [PubMed: 20643349]

9. Alfandari D, Cousin H, Gaultier A, Hoffstrom B, DeSimone D. Integrin α5β1 supports the migration of *Xenopus* cranial neural crest on fibronectin. Developmental Biology. 2003; 260:449–464. [PubMed: 12921745]

10. Wei S, et al. Matrix stiffness drives epithelial–mesenchymal transition and tumour metastasis through a TWIST1–G3BP2 mechanotransduction pathway. Nature Cell Biology. 2015; 17:678–688. [PubMed: 25893917]

11. Sunyer R, et al. Collective cell durotaxis emerges from long-range intercellular force transmission. Science. 2016; 353:1157–1161. [PubMed: 27609894]

12. Koser D, et al. Mechanosensing is critical for axon growth in the developing brain. Nature Neuroscience. 2016; 19:1592–1598. [PubMed: 27643431]

13. Zhou, et al. Actomyosin stiffens the vertebrate embryo during crucial stages of elongation and neural tube closure. Development. 2009; 136:677–688. [PubMed: 19168681]

14. Barriga E, Maxwell P, Reyes A, Mayor R. The hypoxia factor Hif-1α controls neural crest chemotaxis and epithelial to mesenchymal transition. The Journal of Cell Biology. 2013; 201:759–776. [PubMed: 23712262]

15. Rauzi M, Verant P, Lecuit T, Lenne PF. Nature and anisotropy of cortical forces orienting Drosophila tissue morphogenesis. Nature Cell Biology. 2008; 10:1401–1410. [PubMed: 18978783]

16. Bjerke MA, Dzamba B, Wang C, DeSimone DW. FAK is required for tension-dependent organization of collective cell movements in Xenopus mesendoderm. Dev Biol. 2014; 394:340–356. [PubMed: 25127991]

17. Wang N, et al. Mechanical behavior in living cells consistent with the tensegrity model. PNAS. 2001; 98:7765–7770. [PubMed: 11438729]

18. Storm C, Pastore J, MacKintosh F, Lubensky T, Janmey P. Nonlinear elasticity in biological gels. Nature. 2005; 435:191–194. [PubMed: 15889088]

19. Pogoda K, et al. Compression stiffening of brain and its effect on mechanosensing by glioma cells. New Journal of Physics. 2014; 16:075002. [PubMed: 25844043]

20. Charras G, Sahai E. Physical influences of the extracellular environment on cell migration. Nature Reviews Molecular Cell Biology. 2014; 15:813–824. [PubMed: 25355506]

21. Moeendarbary E, et al. The soft mechanical signature of glial scars in the central nervous system. Nat Commun. 2017; 8:14787. [PubMed: 28317912]

22. Chevalier N, et al. How tissue mechanical properties affect enteric neural crest cell migration. Scientific Reports. 2016; 6:20927. [PubMed: 26887292]

23. Seufert D, Hanken J, Klymkowsky M. Type II collagen distribution during cranial development in Xenopus laevis. Anatomy and Embryology. 1994; 189

24. Shindo A, Wallingford J. PCP and Septins Compartmentalize cortical actomyosin to direct collective cell movement. Science. 2014; 343:649–652. [PubMed: 24503851]

25. Koser D, Moeendarbary E, Hanne J, Kuerten S, Franze K. CNS cell distribution and axon orientation determine local spinal cord mechanical properties. Biophysical Journal. 2015; 108:2137–2147. [PubMed: 25954872]

26. Shyer, et al. Emergent cellular self-organization and mechanosensation initiate follicle pattern in the avian skin. Science. 2017; 357:811–815. [PubMed: 28705989]

27. Dzamba, et al. Cadherin Adhesion, Tissue Tension, and Noncanonical Wnt Signaling Regulate Fibronectin Matrix Organization. Developmental Cell. 2009; 16:421–432. [PubMed: 19289087]

28. Webet, et al. A Mechanoresponsive Cadherin-Keratin Complex Directs Polarized Protrusive Behavior and Collective Cell Migration. Developmental Cell. 2012; 22:104–115. [PubMed: 22169071]

29. Wrighton P, Kiessling L. Forces of change: mechanics underlying formation of functional 3D organ buds. Cell Stem Cell. 2015; 16:453–454. [PubMed: 25957897]

30. Poh YC, et al. Generation of organized germ layers from a single mouse embryonic stem cell. Nat Commun. 2014; 5:4000.doi: 10.1038/ncomms5000 [PubMed: 24873804]

31. Mayor R, Morgan R, Sargent M. Induction of the prospective neural crest of Xenopus. Development. 1995; 121:767–777. [PubMed: 7720581]

32. Harland R. In situ hybridization: an improved whole-mount method for Xenopus embryos. Methods Cell Biol. 1991; 36:685–95. [PubMed: 1811161]

33. Mancilla A, Mayor R. Neural Crest Formation in Xenopus laevis: Mechanisms of Xslug Induction. Dev Biol. 1996; 1:580–589.

34. Iioka H, et al. Wnt signalling regulates paxillin ubiquitination essential for mesodermal cell motility. Nature Cell Biology. 2007; 9:813–821. [PubMed: 17558393]

35. Morita H, et al. Cell movements of the deep layer of non-neural ectoderm underlie complete neural tube closure in Xenopus. Development. 2012; 139:1417–1426. [PubMed: 22378637]

36. Weiser D, Row R, Kimelman D. Rho-regulated Myosin phosphatase establishes the level of protrusive activity required for cell movements during zebrafish gastrulation. Development. 2009; 136:2375–2384. [PubMed: 19515695]

37. Kajita M, et al. Interaction with surrounding normal epithelial cells influences signalling pathways and behaviour of Src-transformed cells. Journal of Cell Science. 2009; 123:171–180. [PubMed: 20026643]

38. Theveneau E, Mayor R. Beads on the run: beads as alternative tools for chemotaxis assays. Methods in Molecular Biology. 2011; 769:449–460. [PubMed: 21748694]

39. Hutter J, Bechhoefer J. Calibration of atomic-force microscope tips. Review of Scientific Instruments. 1993; 64:1868–1873.

40. Iwashita M, Kataoka N, Toida K, Kosodo Y. Systematic profiling of spatiotemporal tissue and cellular stiffness in the developing brain. Development. 2014; 141:3793–3798. [PubMed: 25249464]

41. Benko R, Brodland G. Measurement of in vivo stress resultants in neurulation-stage amphibian embryos. Annals of Biomedical Engineering. 2007; 35:672–681. [PubMed: 17237990]

42. Goto T, Davidson L, Ashashima M, Keller R. Planar cell polarity genes regulate polarized extracellular matrix deposition during frog gastrulation. Current Biology. 2005; 15:787–793. [PubMed: 15854914]
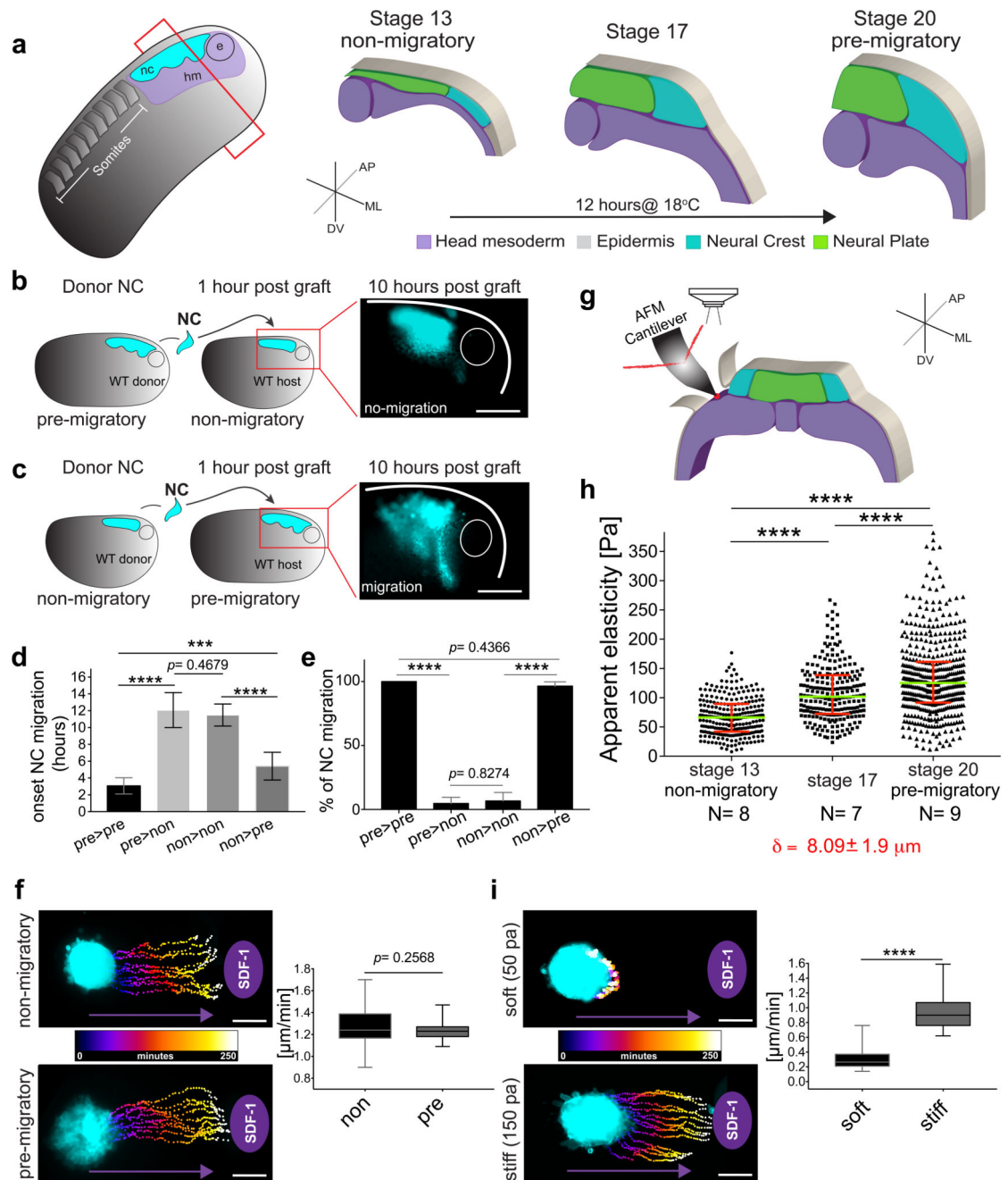
Figure 1. Changes in environmental stiffness are required for neural crest collective migration.
(a) Schematic cross-sections of NC development (AP, anteroposterior; ML, mediolateral; DV dorsoventral). Cephalic NC originates from ectoderm at the border of the neural plate and undergoes EMT before migrating by using head mesoderm as substrate. **(b–e)** Heterochronic grafts. **(b)** Labelled pre-migratory NC (cyan) grafted into non-migratory hosts, a representative example of 'not-migrating' NC at 10 hours post graft is shown. **(c)** Non-migratory NC (cyan) grafted into pre-migratory hosts, a representative example of 'migrating' NC at 10 hours post graft is shown. **(d)** Onset of NC migration. **(e)** Percentage of

migrating NC at 10 hours post graft. Histograms represent media, error bars **(d)** SD, **(e)** s.e.m (one-way ANOVA P<0.0001; two-tailed *t*-test ***P<0.0002, ****P<0.0001, CI= 95%, $N_{b,c,d,e}$ = 43 animals). **(f, i)** Time colour-coded trajectories and speed quantification of NC migrating towards Sdf-1. **(f)** Non-migratory versus pre-migratory NC. **(i)** pre-migratory NC plated on soft or stiff substrates. Boxes in **f,I** represent 25th, median and 75th percentiles, whiskers show spread of data (two-tailed *t*-test, ****P<0.0001, N_f= 78 cells; N_i= 79 cells). **(g–h)** *In vivo* atomic force microscopy (iAFM) measurements. **(g)** iAFM measurement direct on mesoderm**. (i)** Spread of data for each stage, green lines represent median, red whiskers interquartile ranges (two-tailed Mann–Whitney ****P<0.0001, CI= 95%, $n_{stage13}$= 259, $n_{stage17}$= 236, $n_{stage20}$= 461 AFM-indentations, N= number of animals. δ= average indentation depth). Scale bars **(b, c)** 150 μm, **(f, i)** 100 μm. NC, neural crest; e, eye; hm, head mesoderm. **b,c,f,i** representative examples from 3 independent experiments, CI= 95%.
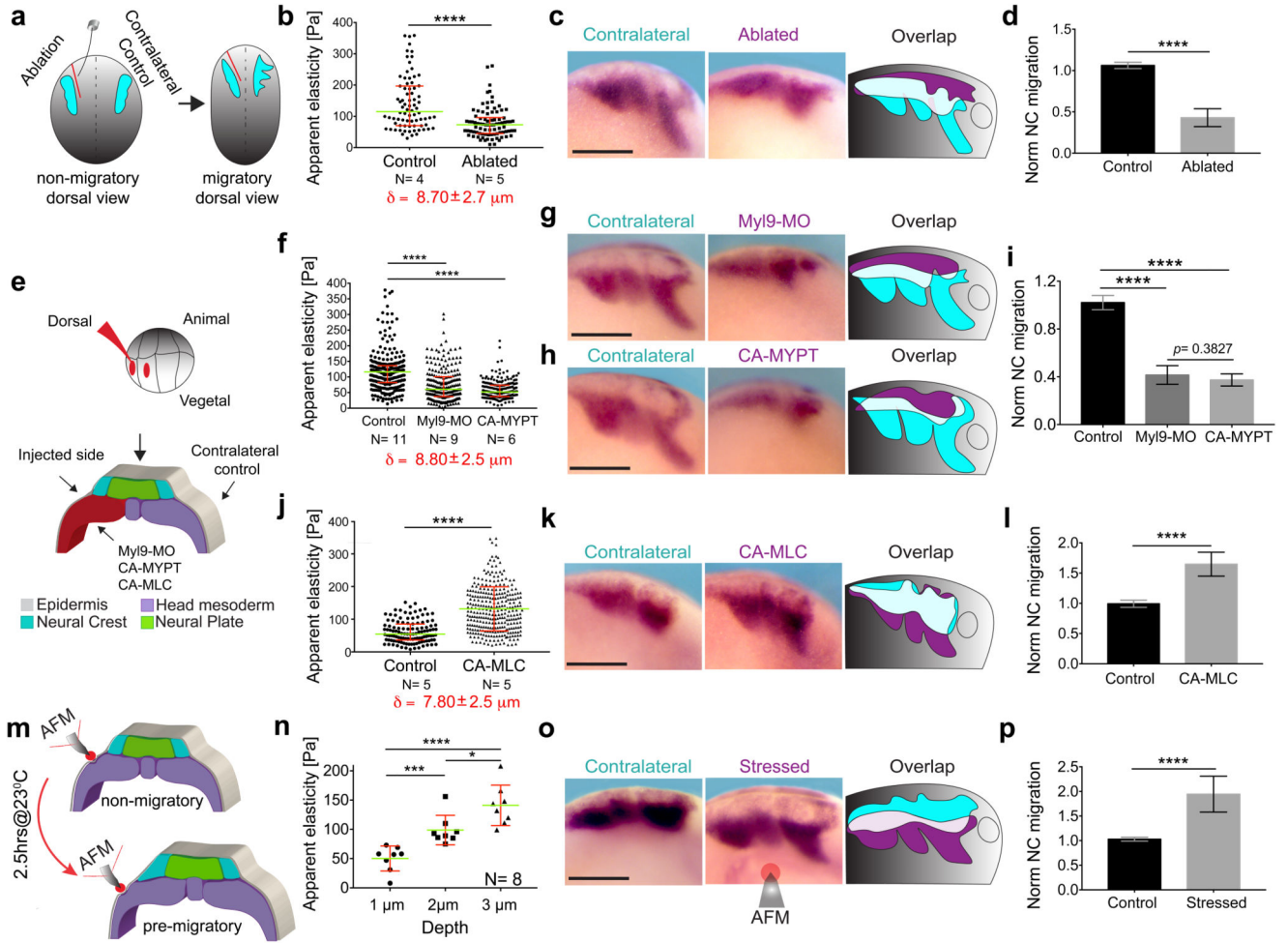
Figure 2. Mesodermal stiffening is essential for neural crest collective migration *in vivo*.
(a–d) Ablation experiments. **(a)** Schematic showing ablation at non-migratory stages, and NC migration at stage-23 (migratory). **(b)** iAFM measurements, n= number of AFM-indentations $n_{control}$= 78, $n_{ablated}$= 86. **(c)** Lateral views of embryos hybridised with a probe against *snail2* to analyse NC migration. **(d)** Normalised NC migration (N_d= 10 animals). **(e–l)** Mesoderm targeted injections. **(e)** Embryos injected into two dorso-vegetal blastomeres (prospective mesoderm). **(f,j)** iAFM measurements. **f,** $n_{control}$= 294, $n_{Myl9-MO}$= 224, $n_{CA-MYPT}$= 223; in **j**, $n_{control}$= 120, n_{CA-MLC}= 301. **(g, h, k)** *snail2*-hybridised embryos. **(i,l)** Normalised NC migration (N_i= 25 animals; N_l=12 animals). **(m–p),** Compression experiments. **(m)** Compression schematics. **(n)** Apparent elasticity plotted as a function of indentation depth, N_n= 8 animals, green lines represent median and whiskers show the spread of data (excluding outliers). **(o)** *snail2*-hybridised embryos. **(p)** Normalised NC migration (N_p= 13 animals). Overlap drawing in **c,g,h,k,o** shown to facilitate comparison of NC migration, control NC (cyan) and treated NC (magenta). **b,f,j** iAFM measurements direct on mesoderm, spread of data; green lines represent median, red whiskers interquartile range (two-tailed Mann–Whitney, ****P<0.0001, CI= 95%, N= number of animals, δ= averaged maximum indentation depths). Histograms in **d,i,l,p** represent media, error bars SD (one-way ANOVA P <0.0001; two-tailed *t*-test *P=0.014, ***P <0.001, ****P<0.0001, CI=

95%). **c,g,h,k,o** representative examples from three independent experiments. Scale bars 200 μm.

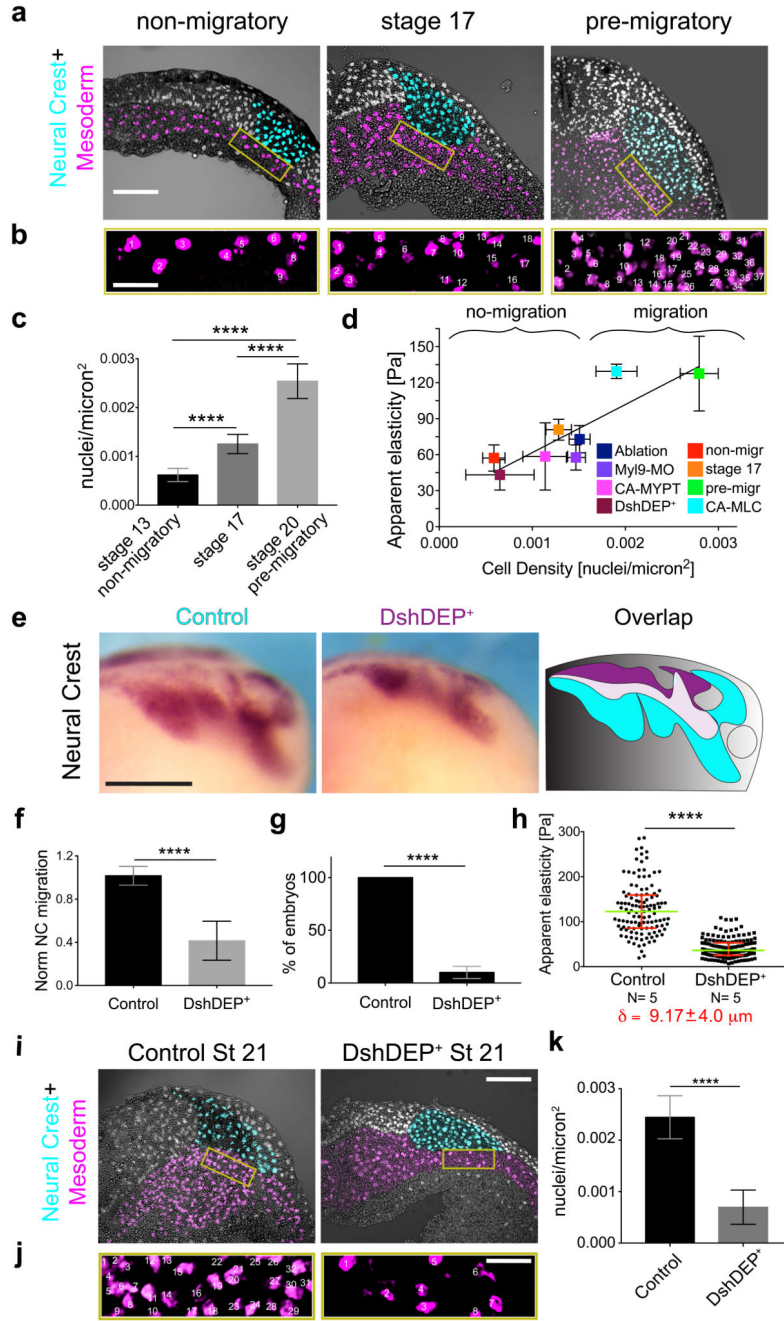**Figure 3. PCP-dependent convergent extension is the driving force for mesodermal stiffening.**
(a–d) Cell density analysis. **(a)** Cross-sections of embryos at the indicated stages showing embryo morphology and pseudo-stained nuclei for NC (cyan) and mesoderm (magenta). **(b)** Magnification of the area used to quantify cell density. **(c)** Nuclei density under the NC (N= 27 sections). **(d)** Head mesoderm apparent elasticity as a function of cell density (Pearson test R= 0.8627, N= 16 animals). **(e–k)** Effect of DshDEP+. **(e)** Lateral views and overlaps of Control (cyan) or DshDEP+ (magenta) *snail2*-hybridised embryos. **(f)** Normalised NC migration (N=14 animals), **(g)** Percentage of embryos. **(h)** iAFM measurement direct on

mesoderm; spread of data, green lines represent median, red whiskers interquartile range (two-tailed Mann–Whitney, ****P<0.0001, CI= 95%, $n_{control}$= 120, n_{DshDEP}^{+}= 148, N= number of animals, δ= averaged maximum indentation depth). **(i)** Overlay showing embryo morphology and nuclei. **(j)** Magnification showing the area used to quantify cell density. **(k)** Nuclei density under the NC, (N= 11 animals). Histograms in **c, f, g, k** represent media, error bars SD, or s.e.m in **g** (one-way ANOVA P <0.0001; two-tailed *t*-test ****P<0.0001, CI= 95%). Scale bars **(a, b, i, j)** 100 μm, **(e)** 200 μm. **a,e,c,f,g,k** representative examples from three independent experiments.
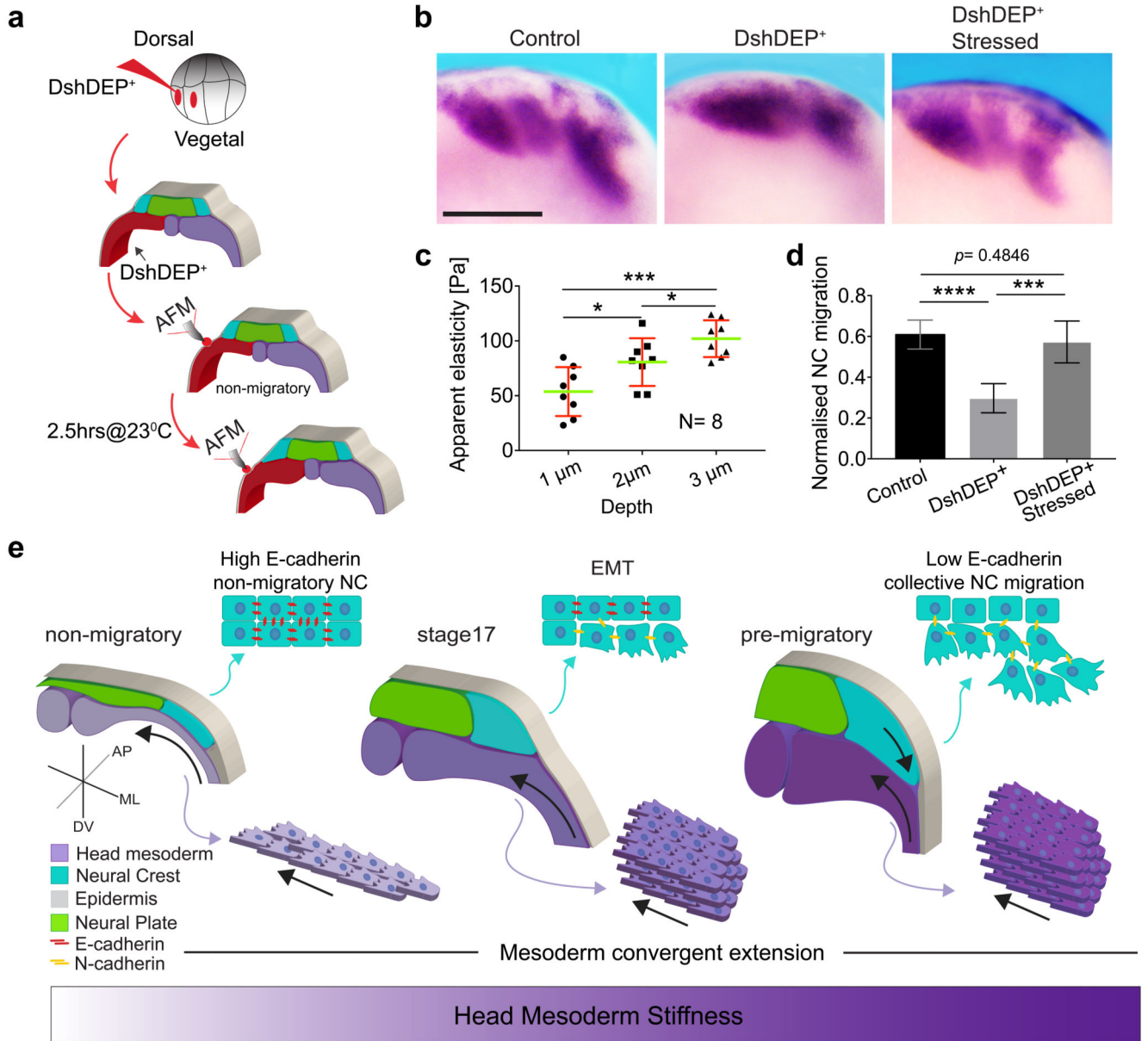
Figure 4. PCP loss-of-function is mechanically rescued by extrinsically inducing mesodermal stiffening.

(**a–d**) Mechanical rescue of DshDEP[+] induced defects. (**a**) Graphic description of compression experiments. (**b**) Lateral view of *snail2*-hybridised embryos. (**c**) Induced apparent elasticity plotted as a function of indentation depth, N_c= 8 animals, green lines represent median and whiskers show the spread of data (excluding outliers). (**d**) Normalised NC migration, N= 19 animals. **b,d** representative examples from three independent experiments. Histograms in **c, d** represent media and error bars SD (one-way ANOVA P <0.0003; two-tailed *t*–test *P<0.045, ***P<0.0002, ****P<0.0001, CI= 95%, δ = average indentation depth. Scale bars (**b**) 200 μm. (**e**) Schematic representing how mechanical interaction between mesoderm and NC coordinates morphogenesis. As convergent extension

progress, the mesoderm stiffens, and in turns, NC epithelial-to-mesenchymal transition (EMT) is triggered and CCM proceed (AP, anteroposterior; ML, mediolateral; DV dorsoventral). NC, Neural crest.